Applied Thermal Engineering 235 (2023) 121347

Contents lists available at ScienceDirect

Applied Thermal Engineering

journal homepage: www.elsevier.com/locate/ate

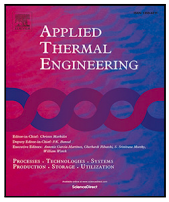

Research Paper

Energy-efficient hybrid model predictive control of mobile refrigeration systems

Markus Fallmann *, Maximilian Lösch, Agnes Poks, Martin Kozek

TU Wien, Institute of Mechanics and Mechatronics, Getreidemarkt 9, 1060 Vienna, Austria

ARTICLE INFO

Keywords:
Hybrid system
Model predictive control
Energy-optimal
Experimental validation
Refrigeration
Door opening

ABSTRACT

Efficiency and temperature compliance of last-mile refrigerated transport suffer from more severe disturbances than stationary applications. The significant energy expenditure and diminished quality or loss of goods have been tackled recently by improved hardware design. However, standard operating strategies only partly use accompanying intrinsic potential. This article introduces an enhanced model predictive control scheme for mobile refrigeration systems with secondary loop cooling units, aiming toward energy-efficient operation complying with temperature restrictions. Its real-time capable optimization covers operational flexibilities and dynamics (storage capacities, door openings, permissible temperature range) more extensively than state-of-the-art solutions. Experimental validation on a specifically designed test rig uses a representative test run with expected and unexpected door openings and a pull-down sequence. A proportional–integral and a standard predictive controller serve for comparison. Performance assessment shows energy savings of 16.4% and improvement in temperature compliance of 3.4% of the advanced predictive over the proportional–integral scheme. If door openings are known upfront, energy consumption decreases by even 29.6%. The standard predictive algorithm shows a similar energy performance but substantially declined temperature compliance as it cannot harness the entire flexibility. Thus, the proposed advanced strategy significantly contributes to more efficient refrigerated transport with reduced environmental impact and loss of goods.

1. Introduction

For modern industrial society, the permanent availability of perishable goods is indispensable. Therefore, reliably maintaining the global cold chain is essential. While non-compliance with temperature limits for a short term merely reduces the quality of food [1], it drives pharmaceutical products completely unusable [2]. With an estimated 1.3 billion tons of food loss yearly caused by insufficient temperature conditions during transport [3], the need for countermeasures becomes plainly visible. In addition to that, the refrigerated transport industry has a significant environmental impact, massively contributing to climate change by accounting for 15% of global fossil fuel consumption [4]. This is further stressed by a yearly increase in the number of refrigerated trucks of 2.5% [5] and the fact that last-mile transportation proves especially challenging due to more substantial variability in operating conditions [6].

This motivates the continuous development of mobile refrigeration toward increased efficiency and more reliable temperature compliance. While, in recent years, much effort was put into hardware design [7,8], little was done regarding operating strategies. Hence, simple on–off approaches still control the majority of classic refrigeration units in commercial applications, yielding low efficiency and shortened life cycles due to high-load operation [9]. An auspicious design regarding efficiency is to extend a classic cooling unit with a thermal storage [6]. While some of those concepts are developed for a highly specialized purpose, e.g., passively acting pre-charged units [10] and energy recovery from the exhaust gas of combustion engines [11], a generally applicable one is the so-called secondary loop configuration [12]. Its high operational safety and flexibility benefit mobile applications [13]. Considering that transported goods practically allow a temperature window rather than demanding a specific reference temperature [14], the flexibility potential of the overall system is even more significant. Nevertheless, state-of-the-art control strategies account for it only partly through heuristics [15,16]. The same holds for door openings, the most severe disturbances in small-scale trucks [17]. Although a classic delivery route comprises 50 door openings on average [18], they are rarely included in the operating strategy, and if so, then only in a rough approximation. All in all, current control approaches only slightly harness the economical and ecological savings potential of state-of-the-art hardware.

* Corresponding author.
E-mail address: markus.fallmann@tuwien.ac.at (M. Fallmann).

https://doi.org/10.1016/j.applthermaleng.2023.121347
Received 4 March 2023; Received in revised form 10 August 2023; Accepted 11 August 2023
Available online 16 August 2023

Nomenclature

Acronyms

D	Time delay of one sample
HMPC	Hybrid model predictive control(ler)
LAN	Local area network
M+S	Measured and sampled
MPC	Model predictive control(ler)
PI	Proportional–integral (controller)
VPN	Virtual private network

Mathematical notation and accents

$\mathcal{N}$	Gaussian distribution
$diag[z_1, \dots, z_n]$	Matrix with elements $z_1, \dots, z_n$ on its diagonal
$\lvert z \rvert$	Absolute value of z
$\lceil z \rceil$	Ceiling of z
$\boldsymbol{z}^{\mathrm{T}}$	Transpose of $\boldsymbol{z}$
$\bar{z}$	Upper validity limit of z
$\underline{z}$	Lower validity limit of z
$\tilde{z}$	Theoretical value of z
$\hat{z}$	Estimate of z
$\dot{z}$	Time derivative of z
z^*	Optimized value of z

Subscripts and superscripts

abs	Absolute
af	Affine
amb	Ambient
b	Binary
c	Continuous
cc	Cooling chamber
cl	Cooling loop
cl/f	Cooling loop and fan
cu	Cooling unit
d	Door/Discrete-time
ec	Energy consumption
exp	Expected
f	Fan
im	Inefficient modes
min/max	Minimum/Maximum
mb	Move blocking
meas	Measured
o	Original
on/off	Up/Down-Time
Q	Heat flow model
red	Reduced
ref	Reference
s	Storage
sm	Smooth
sq	Squared
sub	Sub
tot	Total
tt	Terminal temperature
tw	Temperature window
unexp	Unexpected
w	Wall
wtr	Water
x	State
y	Output

Greek letters

α	Parameters of Peltier submodel
β	Storage heat capacity
γ	Heat transfer coefficient
δ	Slack variable
$\boldsymbol{\Delta}$	Relative to PI
ζ	Parameters of fan submodel
ϑ	Temperature in °C
$\boldsymbol{\theta}$	Parameter vector
κ	Parameters of wall submodel
λ	Parameters of affine approximation
ξ	Parameters of ambient submodel
τ	Minimum up/down-time
χ	Heat capacity of cooling chamber air
ω_{pd}	Pull down switch

Latin letters

a	Eigenvalue
$\boldsymbol{A}$	System matrix
$\boldsymbol{b}$	Manipulated input vector
c	Column
$\boldsymbol{c}$	Column vector
$\boldsymbol{C}$	Output matrix
ctr	Control scheme
d	Disturbance
$\boldsymbol{d}$	Disturbance vector
e	Control error
$\boldsymbol{E}$	Disturbance input matrix
$\boldsymbol{f}$	State equation
f_{MS}	Mode selector function
$\boldsymbol{g}$	Affine vector
$\boldsymbol{I}$	Electrical current
$\boldsymbol{I}$	Identity matrix
$\boldsymbol{J}$	Performance objective
k	Normalized time
K_{p}	Controller gain
l	Approach type
m	Active mode
$\mathcal{M}$	Set of model mode numbers
n	Speed
n_{k}	Total number of time steps within set
N	Number of steps
N_{c}	Length of control horizon
N_{p}	Length of prediction horizon
$\boldsymbol{P}$	Electrical power
$\boldsymbol{P}$	Error covariance matrix
$\dot{\boldsymbol{Q}}$	Heat flow
$\boldsymbol{Q}$	Noise covariance matrix
r	Row
$\boldsymbol{r}$	Row vector
$\boldsymbol{R}$	Weighting factor
s	Switch
S_{tw}	Smoothing factor
$\mathcal{S}$	Test run/Scenario
t	Continuous time
t_{n}	Integration time
t_{s}	Sampling time
$\boldsymbol{T}$	Temperature in K
$\boldsymbol{T}_{\mathrm{mb}}$	Move-blocking matrix
u	Manipulated input
$\boldsymbol{u}$	Vector of manipulated inputs
v	Disturbance input
$\boldsymbol{v}$	Vector of disturbance inputs
V_{ϑ}	Temperature violation
$\boldsymbol{w}$	Vector of noise signals
$\boldsymbol{x}$	State vector of augmented model
$\boldsymbol{y}$	Output vector
$\boldsymbol{z}$	State vector of basic model

This work aims to harness this potential for the refrigeration application of a small-scale truck with a secondary loop cooling unit. For this purpose, a novel model predictive control scheme is presented. In contrast to existing control approaches, full utilization of operational flexibility is enabled by incorporating a holistic model description. The model has been proposed in a preceding work [19] and covers all significant system dynamics and explicitly considers door openings. The model's hybrid mathematical structure is taken into account by means of hybrid model predictive control (HMPC). Based on its well-known theory [20], an appropriately enhanced formulation is introduced, constituting a real-time capable implementation that simultaneously aims toward improved efficiency and temperature compliance. This novel contribution is achieved by introducing a permissible temperature window, a modular objective function additionally considering energy consumption, and constraints reducing the computational burden but sustaining operational flexibility. This advanced control scheme is compared with a standard model predictive approach (MPC) and a logic-based proportional–integral (PI) controller. Validation relies on experimental investigations on a specifically designed test bed, whose dynamic equivalence to a real-world small-scale refrigerated truck has been shown in [21]. The experimental results indicate a satisfying performance and verify substantial improvements in energy consumption and temperature compliance.

Standard model predictive control found its way into industrial applications decades ago [22] and is, therefore, also broadly used in mobile refrigeration applications. In [23], the authors elaborated on a simple linear MPC for a mobile cooling chamber powered by a classic refrigeration unit. Utilized predictions integrate weather forecasts but neglect door openings. Compared with the work presented hereinafter, the simple objective function considers only a specific reference temperature and omits efficiency aspects. Shafiei et al. [24] investigated a refrigerated transport system including a thermal energy storage. Closed-loop simulations with the introduced MPC demonstrate energy savings of approximately 20% when traffic and load predictions are utilized. Attempts to incorporate door openings were made in [25], where the authors considered predefined heat flow trajectories in the optimization problem. They are only valid for a specific opening period and temperature difference between inside and ambient air. To cope with the same problem of different ambient heating conditions, Huang et al. [26] developed a combination of an on–off controller and an MPC for an automotive refrigeration system. Experimental comparisons to standard control approaches proved energy savings of 15.2%. Another work [27] also concentrated on the experimental validation of an MPC that includes heat flow predictions as an approximative remedy. Application of the proposed algorithm on a thermal rig showed potential savings by using an MPC instead of a standard PI controller.

Fundamentally, all these approaches cannot incorporate hybrid model descriptions and, thus, cannot explicitly consider features and available operational flexibilities of the system investigated in this work to their full extent. Therefore, specific research gaps arise from the following considerations. Firstly, to neglect door openings or model them approximately as simple heat flows poorly describe real circumstances and provoke ill-advised control actions, often suboptimally intercepted by heuristics. Furthermore, applying a specific reference temperature rather than a temperature window lapses the associated additional flexibility. Lastly, heuristic consideration of energy consumption impedes a global multi-objective optimization covering efficiency and temperature compliance. All these aspects limit the performance otherwise attainable by system architecture when operated ideally.

Although hybrid model predictive control schemes can consider hybrid models and have been proven promising for various applications [28], the accompanied challenges [29], primarily the high computational complexity, effect that the majority of works focused on simulations only or dynamically slow systems. Besides, hybrid measures in literature only cover refrigeration applications in simple configurations.

In [30], the authors developed a hybrid model predictive control scheme for a supermarket refrigeration system with several display cases. Simulations using a sampling time of 60 s and a horizon length of 10 steps verified a high-efficient operation. Similar performance on the very same plant equipped with classic cooling units was found in simulations by Sarabia et al. [31]. They replaced the mixed-integer optimization problem by solving for switching times instead of switching states at every sampling interval, significantly reducing complexity. More extensive in system structure, Bejarano et al. [32] considered a hybrid approach for a refrigeration system extended by a thermal energy storage based on phase change material. The hybrid formulation covers the different operation modes, i.e., storage charging or discharging. Following a similar storage architecture, others [33] developed an HMPC for cooling electrical consumers in vehicles. A hierarchical configuration eases the computational burden, and a penalty on power consumption in the objective function yields efficient operation. However, the presented simulation results lack comparison with other control approaches. A hierarchical method was also applied by Mork et al. [34], covering a building energy system. The nonlinear plant model is thereby linearized at the beginning of every optimization run. Considering power consumption in the objective function, the HMPC achieves increased efficiency subject to plant-specific restrictions, e.g., minimum up- and down-times. Contrary to the abovementioned works, Ma et al. [35] presented experimental validation of an HMPC. The problem formulation considers an economic objective function extended by a terminal constraint chosen as a robust control invariant set. With an average optimization time of 20 min, the authors achieved 19% efficiency increase for a building cooling system with a stratified thermal storage.

Condensly spoken, the HMPC method, in its basic form presented in the literature above, comes with outstanding matters for the task in this work. Firstly, the high computational burden restricts the application to simple and dynamically slow systems combined with allowed computation times in the minute range. The application investigated hereinafter challenges that in two regards: On the one hand, door openings are highly dynamic and call for rapid response, and on the other hand, the system architecture is regarded as complex compared with published systems handled by HMPC. In summary, holistic system flexibility and features of a refrigerated application with a secondary loop cooling unit and explicit consideration of door openings have never been captured by any (hybrid) model predictive control scheme in the literature. Secondly, even for comparably simple systems, HMPC operation is rarely validated using real-world experiments. For the better part, only simulations indicate significant improvements over other control techniques. However, missing real-world validation limits the results' significance.

Arising research gaps are addressed by this work, comprising the following novel contributions within the scope of refrigeration control:

- Real-time capable HMPC concept for a mobile refrigeration application utilizing the entire operational dynamics and flexibility (storage capacity of wall insulation, storage capacity in secondary loop refrigeration unit, independent charging/discharging of storage loop, door openings, permissible temperature range) to improve efficiency and temperature compliance.
- Experimental verification of performance increase due to holistic and explicit consideration of system dynamics, done via HMPC, over simplified approaches, i.e., PI and MPC.

The remainder of the paper is structured as follows: Section 2 outlines the system architecture and its test bed counterpart. Then, elaborations on different model formulations and their parameterization in Section 3 are followed by detailed explanations on control design in Section 4. The experimental setup is introduced in Section 5. Next, Section 6 elaborates on experimental results and performance assessment. The work ends with a discussion in Section 7 and a conclusion in Section 8.

2. System description

The original system under consideration covers the entire refrigeration application of a small-scale truck, see Fig. 1 a. This setup is commercially available and equipped with a secondary loop refrigeration unit manufactured by PBX GmbH [36].

The cooling chamber is strongly insulated, serving two purposes: inhibiting the effect of the ambient temperature $\vartheta_{amb} \in \mathbb{R}$ on the air inside and acting as a thermal storage to rapidly smooth the impact of short-term disturbances. However, door openings (door status $s_d \in \{0, 1\}$) constitute severe disruptions [18] as they evoke significant heat and mass transfer [17]. Deliberate temperature influence originates from a classic cooling loop using propane as its coolant. It is connected to the cooling chamber by a single-phase storage loop filled with a water-glycol mixture. On the one hand, this architecture rules out any chance of propane contaminating the cooling chamber and, on the other hand, provides storage capacity that enables improved overall efficiency if appropriately operated [12,13]. While the cooling loop heat flow $\dot{Q}_{cl} \in \mathbb{R}$ depends on the cooling loop switch $s_{cl} \in \{0, 1\}$ and the compressor speed $n_{cl} \in \mathbb{R}$ and charges the storage by decreasing its temperature $\vartheta_s \in \mathbb{R}$, the fan switch $s_f \in \{0, 1\}$ determines whether natural or forced convection effects the discharging heat flow. Eventually, the cooling unit heat flow $\dot{Q}_{cu} \in \mathbb{R}$, influences the temperature of the air inside the cooling chamber. As shown in [37], the chamber's compact design allows for characterizing it by a single value, namely $\vartheta_{cc} \in \mathbb{R}$.

Reproducible, high-quality experimental investigations on the original system are costly and require large-scale equipment. Since control-related analyses merely call for holistic system considerations, this work utilizes a simplified test bed setup (Fig. 1 b). The cooling chamber is geometrically similar but smaller and insulated in such a way as to ensure the same heat transfer coefficient. Furthermore, an aluminum heat sink constitutes the thermal storage, and a Peltier element [38] emulates the cooling loop. Thus, the compressor speed as the manipulated continuous input is replaced by the Peltier current $I_{cl} \in \mathbb{R}$. Besides, fresh water cooling ensures sufficient dissipation of occurring waste heat, keeping the heat exchanger water temperature $\vartheta_{wtr} \in \mathbb{R}$ constant. Although both setups possess apparent structural differences, qualitative dynamics are identical, as shown in [21].

3. Model description

Because binary quantities influence the system dynamics in a switching fashion, hybrid modeling is the method of choice [20]. The hybrid modeling framework is generally beneficial when discrete events trigger a change in system dynamics. The essence is a set of continuous, time-invariant state–space formulations covering dynamically different

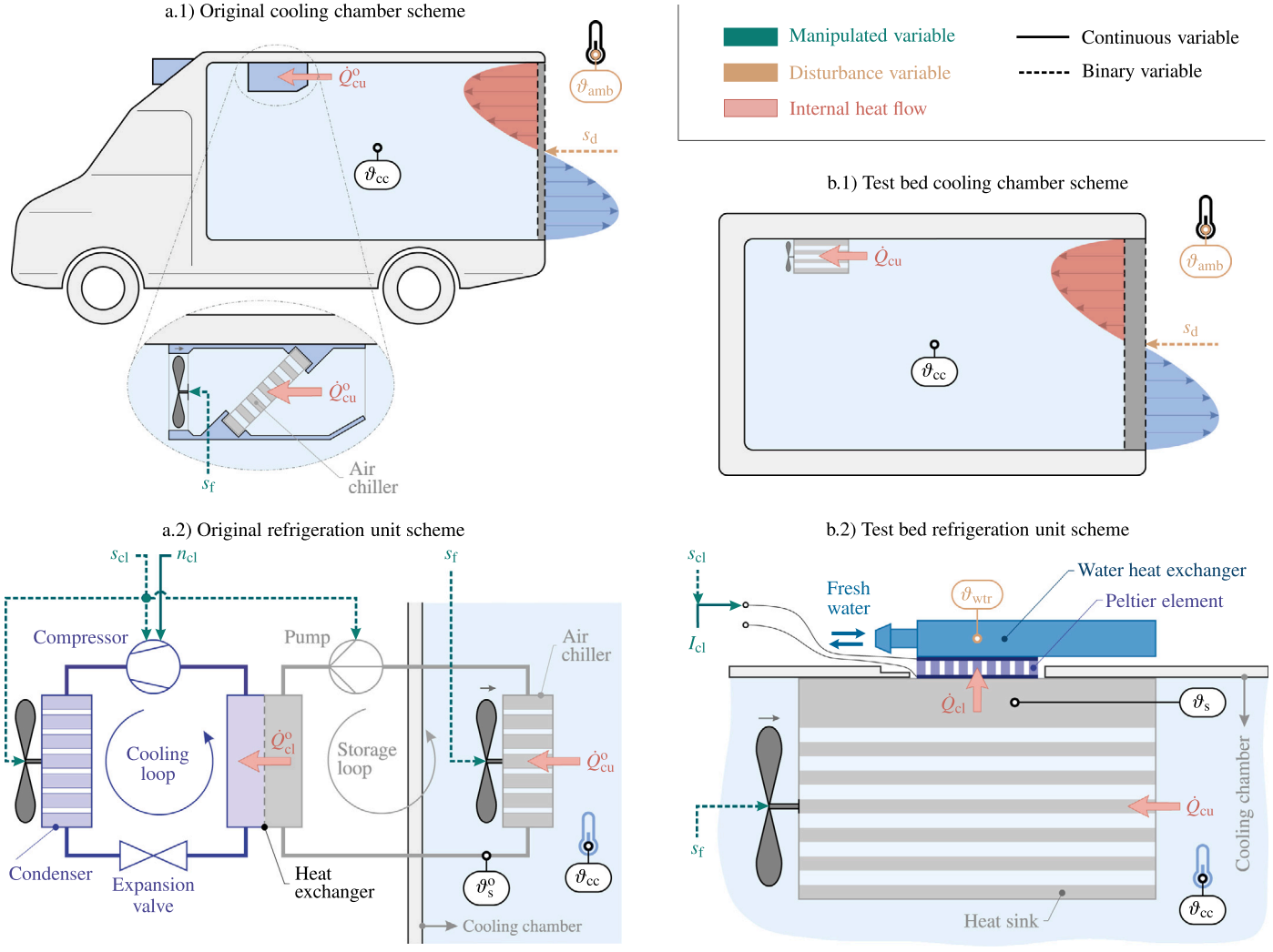

Fig. 1. Schematic illustration of (a.1) the small-scale refrigerated truck with (a.2) its secondary loop refrigeration unit and (b) their test bed counterparts. Small arrows above fans indicate associated airflow directions, and a superscript "o" highlights quantities affected by significantly different structures in the original and test bed setup. *Binary inputs*: door status s_d, cooling loop switch s_{cl}, fan switch s_f. *Continuous inputs*: compressor speed n_{cl}, Peltier current I_{cl}. *Heatflow*: cooling loop heat flow $\dot{Q}_{cl}$, cooling unit heat flow $\dot{Q}_{cu}$. *Temperatures*: ambient air ϑ_{amb}, air inside cooling chamber ϑ_{cc}, storage ϑ_s.

operating conditions. With a combination of binary variables representing the current condition, the corresponding state–space model is selected. In brief, binary inputs choose the specific dynamics on which continuous inputs act. A graphical illustration of the very modeling framework used throughout this work can be found in [19].

Different design tasks require tailor-made model formulations. Emerging from a basic first-principles version (Section 3.1), a nonlinear observer and affine control design model are deduced in Sections 3.2 and 3.3, respectively.

3.1. Basic nonlinear hybrid model

In a previous work [19], the authors elaborated on a hybrid nonlinear model for the original system and experimentally verified its applicability. In the following, the equations presented therein will be adapted to fit the test bed (Fig. 1 b). Note the conversion for any temperature quantity used throughout this work according to

$$T = \vartheta + 273.15, \tag{1}$$

where $T \in \mathbb{R}_{\geq 0}$ is given in K and $\vartheta \in \mathbb{R}$ in °C.

Substituting the classic cooling loop with a Peltier element is the main difference. Using a simple energy equilibrium approach [38,39] yields the heat flow according to

$$\dot{Q}_{\mathrm{cl}}(t) = \left[\alpha_1\, I_{\mathrm{cl}}(t)\, T_{\mathrm{s}}(t) - \alpha_2\, I_{\mathrm{cl}}^2(t) - \alpha_3 \left[T_{\mathrm{wtr}}(t) - T_{\mathrm{s}}(t)\right]\right] s_{\mathrm{cl}}(t) \tag{2}$$

and the associated cooling loop power demand $P_{\mathrm{cl}} \in \mathbb{R}_{\geq 0}$ as

$$P_{\mathrm{cl}}(t) = \left[\alpha_1 \left[T_{\mathrm{wtr}}(t) - T_{\mathrm{s}}(t)\right] I_{\mathrm{cl}}(t) + 2\,\alpha_2\, I_{\mathrm{cl}}^2(t)\right] s_{\mathrm{cl}}(t), \tag{3}$$

where $\alpha_i \in \mathbb{R}_{\geq 0}$, $i \in \{1,2,3\}$ label unknown parameters. The storage's energy balance is given by

$$\beta \frac{d}{dt} T_{\mathrm{s}}(t) = -\dot{Q}_{\mathrm{cl}}(t) + \dot{Q}_{\mathrm{cu}}(t) \tag{4}$$

with the heat capacity $\beta \in \mathbb{R}_{\geq 0}$, remaining unaltered to [19]. The same holds for

$$\dot{Q}_{\mathrm{cu}}(t) = \left[T_{\mathrm{cc}}(t) - T_{\mathrm{s}}(t)\right] \left[\gamma_1\, s_{\mathrm{f}}(t) + \gamma_2 \left[1 - s_{\mathrm{f}}(t)\right]\right], \tag{5}$$

where $\gamma_1 \in \mathbb{R}_{\geq 0}$ and $\gamma_2 \in \mathbb{R}_{\geq 0}$ label the heat transfer coefficient related to forced and natural convection, respectively. Another difference to the original model relates to the computational burden of predictive control schemes. To keep them at bay, not two but just one thermal mass represents the insulated wall. Besides, the modeled wall degenerates to a thermal capacity merely interacting with the air inside. The evolution of the wall temperature $T_{\mathrm{w}} \in \mathbb{R}_{\geq 0}$ is then given as

$$\kappa_1 \frac{d}{dt} T_{\mathrm{w}}(t) = \kappa_2 \left[T_{\mathrm{cc}}(t) - T_{\mathrm{w}}(t)\right] = \dot{Q}_{\mathrm{w}}(t), \tag{6}$$

where $\kappa_1 \in \mathbb{R}_{\geq 0}$ is its heat capacity, $\kappa_2 \in \mathbb{R}_{\geq 0}$ the heat transfer coefficient, and $\dot{Q}_{\mathrm{w}} \in \mathbb{R}$ the exchanged heat flow. With those simplifications, the heat flow due to ambient conditions, $\dot{Q}_{\mathrm{amb}} \in \mathbb{R}$, can be written as

$$\dot{Q}_{\mathrm{amb}}(t) = \xi_1 \left[T_{\mathrm{amb}}(t) - T_{\mathrm{cc}}(t)\right] + \xi_2 \left[T_{\mathrm{amb}}(t) - T_{\mathrm{cc}}(t)\right] s_{\mathrm{d}}(t) \tag{7}$$

with the unknown parameters $\xi_i \in \mathbb{R}_{\geq 0}$, $i \in \{1,2\}$. Eventually, the evolution of the temperature inside the chamber obeys

$$\chi \frac{d}{dt} T_{\mathrm{cc}}(t) = -\dot{Q}_{\mathrm{cu}}(t) + P_{\mathrm{f}}(t) + \dot{Q}_{\mathrm{amb}}(t) - \dot{Q}_{\mathrm{w}}(t), \tag{8}$$

where $\chi \in \mathbb{R}_{\geq 0}$ labels the air-related heat capacity, and $P_{\mathrm{f}} \in \mathbb{R}_{\geq 0}$ is the fan power demand given by

$$P_{\mathrm{f}}(t) = \zeta\, s_{\mathrm{f}}(t) \tag{9}$$

with the unknown parameter $\zeta \in \mathbb{R}_{\geq 0}$. Thus, the total cooling unit power demand $P_{\mathrm{cu}} \in \mathbb{R}_{\geq 0}$ results as

$$P_{\mathrm{cu}}(t) = P_{\mathrm{cl}}(t) + P_{\mathrm{f}}(t). \tag{10}$$

In order to gain a sensible compact description, the model inputs are assembled as binary manipulated inputs $\boldsymbol{u}_{\mathrm{b}} \in \{0,1\}^2$, binary disturbance inputs $v_{\mathrm{b}} \in \{0,1\}$, continuous manipulated inputs $u_{\mathrm{c}} \in \mathbb{R}$, and continuous disturbance inputs $\boldsymbol{v}_{\mathrm{c}} \in \mathbb{R}^2$:

$$\boldsymbol{u}_{\mathrm{b}}(t) := \left[s_{\mathrm{cl}}(t),\ s_{\mathrm{f}}(t)\right]^{\mathrm{T}} \tag{11a}$$

$$v_{\mathrm{b}}(t) := s_{\mathrm{d}}(t) \tag{11b}$$

$$u_{\mathrm{c}}(t) := I_{\mathrm{cl}}(t) \tag{11c}$$

$$\boldsymbol{v}_{\mathrm{c}}(t) := \left[T_{\mathrm{amb}}(t),\ T_{\mathrm{wtr}}(t)\right]^{\mathrm{T}} \tag{11d}$$

With the state vector $\boldsymbol{z}_{\mathrm{c}} \in \mathbb{R}^3$ given as

$$\boldsymbol{z}_{\mathrm{c}}(t) := \left[T_{\mathrm{s}}(t),\ T_{\mathrm{cc}}(t),\ T_{\mathrm{w}}(t)\right]^{\mathrm{T}}, \tag{12}$$

the output vector $\boldsymbol{y}_{\mathrm{c}} \in \mathbb{R}^2$ defined as

$$\boldsymbol{y}_{\mathrm{c}}(t) := \left[T_{\mathrm{s}}(t),\ T_{\mathrm{cc}}(t)\right]^{\mathrm{T}}, \tag{13}$$

and the parameter vector $\boldsymbol{\theta} \in \mathbb{R}_{\geq 0}^{12}$ given by

$$\boldsymbol{\theta} = \left[\alpha_1, \alpha_2, \alpha_3, \beta, \gamma_1, \gamma_2, \zeta, \kappa_1, \kappa_2, \xi_1, \xi_2, \chi\right]^{\mathrm{T}}, \tag{14}$$

the continuous system dynamics can be written according to:

$$\dot{\boldsymbol{z}}_{\mathrm{c}}(t;\boldsymbol{\theta}) = \boldsymbol{f}\left(\boldsymbol{z}_{\mathrm{c}}(t), u_{\mathrm{c}}(t), \boldsymbol{v}_{\mathrm{c}}(t); m(t), \boldsymbol{\theta}\right) \tag{15a}$$

$$\boldsymbol{y}_{\mathrm{c}}(t) = \boldsymbol{C}\, \boldsymbol{z}_{\mathrm{c}}(t) \tag{15b}$$

Thereby, $\boldsymbol{f} : \mathbb{R}^6 \times \{0,1\}^3 \to \mathbb{R}^3$ labels the state equation, $\boldsymbol{C}$ is the output matrix given as

$$\boldsymbol{C} = \begin{bmatrix} 1 & 0 & 0 \\ 0 & 1 & 0 \end{bmatrix}, \tag{16}$$

and $m(t) \in \mathcal{M} = \{1,2,\ldots,8\}$ labels the currently active model mode defined by the mode selector $f_{\mathrm{MS}} : \{0,1\}^3 \to \mathcal{M}$. The relation is stated in detail in Table 1 and can be written compactly as

$$m(t) = f_{\mathrm{MS}}\left(s_{\mathrm{cl}}(t), s_{\mathrm{f}}(t), s_{\mathrm{d}}(t)\right). \tag{17}$$

Based on the binary inputs, the mode selector (17) defines which specific nonlinear continuous model out of the switched dynamics (15) is currently active. Together, they represent the hybrid model, to be more precise, a degenerated form of a discrete hybrid automaton [20]. From now on, the $\boldsymbol{\theta}$-dependency of (15) will be omitted for brevity. For parameterization, see Section 3.4.

Table 1
Classification of the currently active model mode depending on the cooling loop switch s_{cl}, the fan switch s_{f}, and door opening status s_{d}. While 0 indicates that the respective part is off or the door is closed, a value of 1 represents an active part or an open door.

Mode $m(t)$	$s_{\mathrm{cl}}(t)$	$s_{\mathrm{f}}(t)$	$s_{\mathrm{d}}(t)$
1	0	0	0
2	1	0	0
3	0	1	0
4	1	1	0
5	0	0	1
6	1	0	1
7	0	1	1
8	1	1	1

3.2. Augmented nonlinear hybrid model

It is well-known that unavoidable model mismatches cause steady-state offsets when optimal control problems rely on deterministic model formulations [20,22]. Augmenting the basic formulation with a disturbance model is a state-of-the-art remedy. A state observer then maps occurring deviations into disturbance estimates, allowing predictive control schemes to attain offset-free steady-state operation.

Many different design approaches exist in literature [40], but a lack of detailed insight into unmodeled effects in this work favors

a simple, generally applicable approach for augmenting the switched dynamics (15):

$$\dot{\boldsymbol{x}}_\mathrm{c}(t) = \boldsymbol{f}\left(\boldsymbol{x}_\mathrm{c}(t), u_\mathrm{c}(t), \boldsymbol{v}_\mathrm{c}(t); m(t)\right) + \boldsymbol{w}_\mathrm{x}(t) \tag{18a}$$

$$\dot{\boldsymbol{d}}(t) = \boldsymbol{w}_\mathrm{d}(t) \tag{18b}$$

$$\boldsymbol{y}_\mathrm{c}(t) = \boldsymbol{C}\,\boldsymbol{x}_\mathrm{c}(t) + \boldsymbol{d}(t) + \boldsymbol{w}_\mathrm{y}(t) \tag{18c}$$

Thereby, the storage disturbance $d_\mathrm{s} \in \mathbb{R}$ and cooling chamber disturbance $d_\mathrm{c} \in \mathbb{R}$, aggregated as the disturbance vector $\boldsymbol{d} \in \mathbb{R}^2$ according to

$$\boldsymbol{d}(t) = \left[d_\mathrm{s}(t),\ d_\mathrm{cc}(t)\right]^\mathrm{T}, \tag{19}$$

act directly upon the outputs. The process noise $\boldsymbol{w}_\mathrm{x} \in \mathbb{R}^3$, disturbance noise $\boldsymbol{w}_\mathrm{d} \in \mathbb{R}^2$, and measurement noise $\boldsymbol{w}_\mathrm{y} \in \mathbb{R}^2$ complete the augmentation and are given as

$$\boldsymbol{w}_\mathrm{x}(t) \sim \mathcal{N}\left(\boldsymbol{0}, \boldsymbol{Q}_\mathrm{x}\right),\ \boldsymbol{w}_\mathrm{d}(t) \sim \mathcal{N}\left(\boldsymbol{0}, \boldsymbol{Q}_\mathrm{d}\right),\ \boldsymbol{w}_\mathrm{y}(t) \sim \mathcal{N}\left(\boldsymbol{0}, \boldsymbol{Q}_\mathrm{y}\right), \tag{20}$$

where $\boldsymbol{Q}_i$, $i \in \{\mathrm{x}, \mathrm{d}, \mathrm{y}\}$ label associated covariance matrices.

With those extensions, the model states no longer correspond to the lumped temperatures as in (12), indicated in (18) by using the modified symbol $\boldsymbol{x}_\mathrm{c}$ for model states. However, if considered without noise ($\boldsymbol{w}_\mathrm{y} = \boldsymbol{0}$), states can be interpreted as shifted temperatures:

$$\begin{aligned}\boldsymbol{x}_\mathrm{c}(t) :=& \left[x_{\mathrm{c},1}(t),\ x_{\mathrm{c},2}(t),\ x_{\mathrm{c},3}(t)\right]^\mathrm{T} = \cdots \\ & \left[T_\mathrm{s}(t) - d_\mathrm{s}(t),\ T_\mathrm{cc}(t) - d_\mathrm{cc}(t),\ T_\mathrm{w}(t)\right]^\mathrm{T}\end{aligned} \tag{21}$$

3.3. Augmented affine hybrid model

Although the switched nonlinear dynamics (18) appropriately fulfill observer needs, its complexity raises significant computational difficulties when utilized in optimal control problems. Here, an affine, deterministic formulation alleviates the computational burden.

The only continuous nonlinearity arises from parts of the cooling loop heat flow (2), namely the here-called sub heat flow $\dot{Q}_\mathrm{sub} \in \mathbb{R}$ given by

$$\dot{Q}_\mathrm{sub}(T_\mathrm{s}, I_\mathrm{cl}) = \alpha_1\, I_\mathrm{cl}\, T_\mathrm{s} - \alpha_2\, I_\mathrm{cl}^2. \tag{22}$$

The specific formulation of the optimal control problem (see Section 4.3) demands two different affine approximations $\dot{Q}_\mathrm{sub}^\mathrm{af} \in \mathbb{R}$ according to

$$\dot{Q}_\mathrm{sub}^\mathrm{af}(T_\mathrm{s}, I_\mathrm{cl}; l) = \begin{cases} \lambda_1\, T_\mathrm{s} + \lambda_2\, I_\mathrm{cl} - \lambda_3 & \dots\ l = 1 \\ \lambda_4\, I_\mathrm{cl} & \dots\ l = 0, \end{cases} \tag{23}$$

where $\lambda_i \in \mathbb{R}_{\geq 0}$, $i \in \{1, 2, 3, 4\}$ are unknown coefficients and $l \in \{0, 1\}$ indicates the approach type. As depicted in Fig. 2, type "$l = 1$" comes with a lower current limit and considers the T_s-dependency, and type "$l = 0$" covers a current span starting at 0 and averages over the entire temperature range. The chosen type depends on whether local accuracy at high current values or a broad validity range is predominantly essential.

Based on (18), neglecting the noise processes to gain a deterministic description and applying the substitute $\dot{Q}_\mathrm{sub} \leftarrow \dot{Q}_\mathrm{sub}^\mathrm{af}$ yields the switched affine dynamics as follows:

$$\dot{\boldsymbol{x}}_\mathrm{c}(t) = \boldsymbol{A}(m, l)\,\boldsymbol{x}_\mathrm{c}(t) + \boldsymbol{b}(m, l)\,u_\mathrm{c}(t) + \boldsymbol{E}(m)\,\boldsymbol{v}_\mathrm{c}(t) + \boldsymbol{g}(m, l) \tag{24a}$$

$$\dot{\boldsymbol{d}}(t) = \boldsymbol{0} \tag{24b}$$

$$\boldsymbol{y}_\mathrm{c}(t) = \boldsymbol{C}\,\boldsymbol{x}_\mathrm{c}(t) + \boldsymbol{d}(t) \tag{24c}$$

Thereby, $\boldsymbol{A} \in \mathbb{R}^{3\times3}$ labels the system matrix, $\boldsymbol{b} \in \mathbb{R}^3$ the manipulated input vector, $\boldsymbol{E} \in \mathbb{R}^{3\times2}$ the disturbance input matrix, and $\boldsymbol{g} \in \mathbb{R}^3$ the affine vector. For brevity, time dependencies of m and l are omitted.

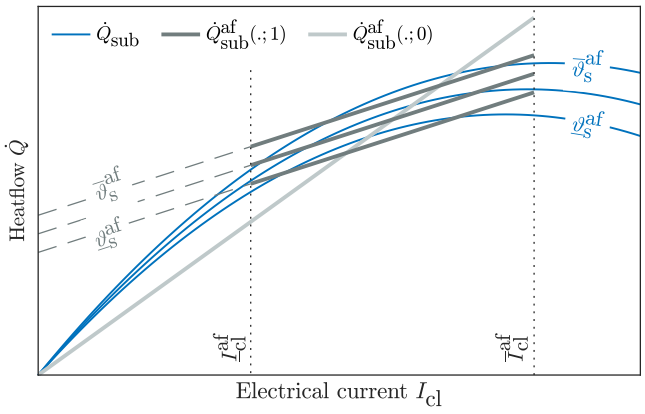

Fig. 2. Schematic illustration of the two affine approximations $\dot{Q}_\mathrm{sub}^\mathrm{af}$ (23) of the nonlinear sub heat flow $\dot{Q}_\mathrm{sub}$ (22) and lower and upper limits, i.e., $\underline{(.)}^\mathrm{af}$ and $\bar{(.)}^\mathrm{af}$, utilized for parameterization. Compared with type "1", type "0" neglects temperature dependency and ensures zero input current results in zero heat flow.

3.4. Parameterization

The determination of model parameters $\boldsymbol{\theta}$ (14) relies on open-loop experiments of the test bed and the estimation procedure described in [19]. Based on evaluating the parameterized nonlinear heat flow model (22) at a series of points evenly distributed within the chosen validity ranges, the coefficients of the affine approaches (23) are estimated using least squares method [41].

4. Control design

The control objective unifies two contradictory goals: Keeping the cooling chamber temperature within a specific temperature window while minimizing overall energy consumption. This work strives for this holistically by adopting and enhancing the basic concept of hybrid model predictive control [20]. Besides, its performance will be compared to a standard model predictive scheme deduced by applying vast simplifications. A proportional–integral controller serves as an additional reference.

From now on, for the sake of brevity, continuous and binary quantities are aggregated into generalized manipulated inputs $\boldsymbol{u}$ and disturbance inputs $\boldsymbol{v}$ according to:

$$\boldsymbol{u}(.) := \left[u_\mathrm{c}(.),\ \boldsymbol{u}_\mathrm{b}^\mathrm{T}(.)\right]^\mathrm{T},\quad \boldsymbol{v}(.) := \left[\boldsymbol{v}_\mathrm{c}^\mathrm{T}(.),\ v_\mathrm{b}(.)\right]^\mathrm{T} \tag{25}$$

As depicted in Fig. 3, the algorithms representing the extended controller determine the reference (superscript *ref*) for the manipulated input vector based on measured values (superscript *meas*). Note that these superscripts are only stated if necessary to avoid ambiguities. Compared with the PI, both predictive schemes use information on expected future door openings, $s_\mathrm{d}^\mathrm{exp}$, and depend on an observer to overcome the partial measurability of model states and to ensure steady-state offset-free operation. With all algorithms being digitally implemented, they run a computation at every normalized time $k \in \mathbb{N}_0$, $k = t/t_\mathrm{s}$, where $t_\mathrm{s} \in \mathbb{R}_{>0}$ is the sampling time.

Besides pursuing the control objective, all algorithms must ensure operational compliance with system-specific limitations:

(a) Following compressor speed limits in the original system (Fig. 1 a), the cooling loop current must be kept between a lower and upper bound:

$$I_\mathrm{cl}^\mathrm{min} \leq I_\mathrm{cl}(t) \leq I_\mathrm{cl}^\mathrm{max} \tag{26}$$

(b) Minimum up(on)- and down(off)-times $\tau_i^j \in \mathbb{R}_{\geq 0}$, $i \in \{\mathrm{cl},\mathrm{f}\}$, $j \in \{\mathrm{on},\ \mathrm{off}\}$ of the cooling loop and fan must be obeyed. For the digital implementation, minimum times are transformed into minimum time steps $N_i^j \in \mathbb{N}_0$ according to:

$$N_{\{\mathrm{cl},\ \mathrm{f}\}}^{\{\mathrm{on},\ \mathrm{off}\}} = \left\lceil \tau_{\{\mathrm{cl},\ \mathrm{f}\}}^{\{\mathrm{on},\ \mathrm{off}\}} / t_\mathrm{s} \right\rceil \tag{27}$$

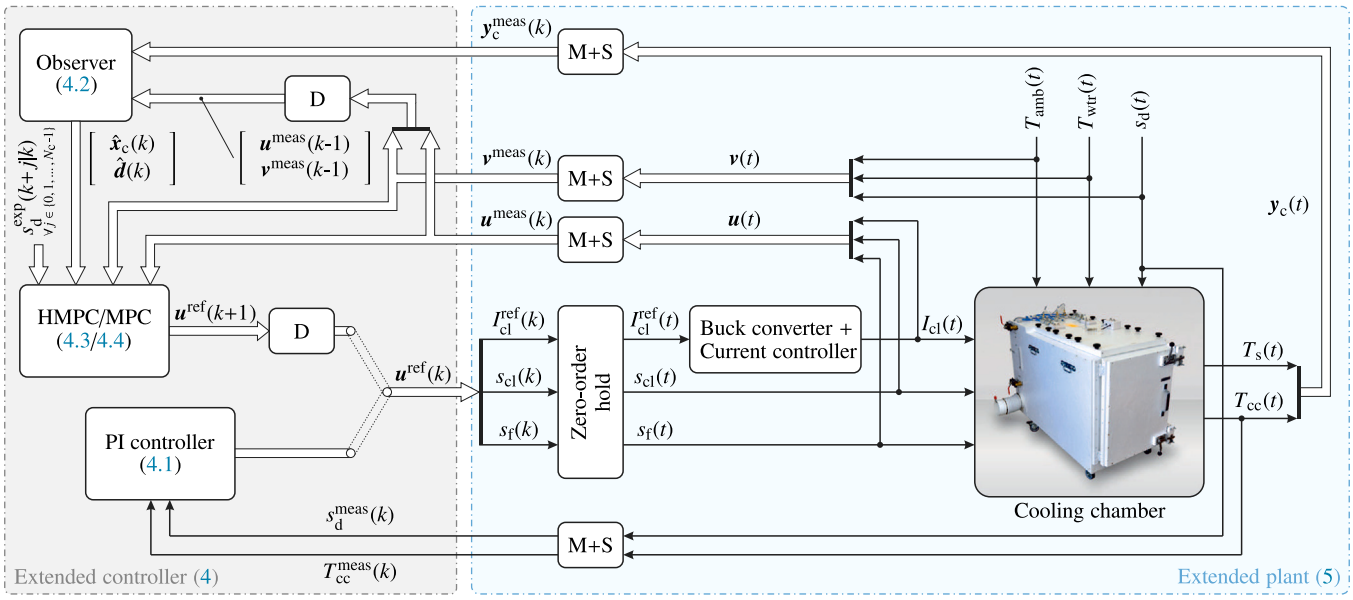

Fig. 3. Conceptual architecture of the overall control structure. The extended controller determines reference values for the manipulated inputs, relying on measured and sampled (M+S) quantities. Within the extended plant, a subjacent controller driving a buck converter realizes the current reference. The abbreviation D indicates a time delay of one sample, and numbers in brackets refer to sections with detailed explanations.

4.1. Proportional–integral controller

More precisely, the proposed algorithm is a rule-based hysteresis proportional–integral controller. Since many commercially available mobile refrigeration applications still use simple on–off controllers [42], the one used here represents an advanced industrial standard [9,43] and, therefore, allows a sensible comparison.

The chosen approach actuates the cooling loop and fan switch together, i.e., it only has to determine a single binary input, the operating switch $s_{\mathrm{cl/f}} \in \{0, 1\}$, for which

$$s_{\mathrm{cl/f}}(k) = s_{\mathrm{cl}}(k) = s_{\mathrm{f}}(k), \quad \forall k \in \mathbb{N}_0 \tag{28}$$

holds. Therefore, the combined minimum up- and down-times are given as

$$N_{\mathrm{cl/f}}^{\{\mathrm{on,\ off}\}} = \max\left(N_{\mathrm{cl}}^{\{\mathrm{on,\ off}\}}, N_{\mathrm{f}}^{\{\mathrm{on,\ off}\}}\right). \tag{29}$$

Since complying with these restrictions is essential, the algorithm considers them up front (Fig. 4).

Based on the operating switch in the preceding time step, it either checks the down-time condition

$$s_{\mathrm{cl/f}}(k\text{-}j) = 0, \quad \forall j \in \left\{1, 2, \dots, N_{\mathrm{cl/f}}^{\mathrm{off}}\right\} \tag{30}$$

or up-time condition

$$s_{\mathrm{cl/f}}(k\text{-}j) = 1, \quad \forall j \in \left\{1, 2, \dots, N_{\mathrm{cl/f}}^{\mathrm{on}}\right\}. \tag{31}$$

On the second-highest priority level, the efficiency condition impedes enforced interaction with the environment by shutting down the unit when the door is open. If the operation switch remains indefinite after checking the above conditions, a switching hysteresis with the lower and upper bounds of the temperature window, $T_{\mathrm{tw}}^{\mathrm{min}}$ and $T_{\mathrm{tw}}^{\mathrm{max}}$, becomes active. For an eventually activated unit, the current reference value $I_{\mathrm{cl}}^{\mathrm{ref}}$ results from a simple PI law given as

$$e(k) = T_{\mathrm{cc}}^{\mathrm{ref}} - T_{\mathrm{cc}}^{\mathrm{meas}}(k) \tag{32a}$$

$$\tilde{I}_{\mathrm{cl}}^{\mathrm{ref}}(k) = I_{\mathrm{cl}}^{\mathrm{ref}}(k\text{-}1) + K_{\mathrm{p}}\, e(k) + K_{\mathrm{p}}\left(-1 + t_{\mathrm{s}}/t_{\mathrm{n}}\right) e(k\text{-}1) \tag{32b}$$

$$I_{\mathrm{cl}}^{\mathrm{ref}}(k) = \max\left(I_{\mathrm{cl}}^{\mathrm{min}}, \min\left(I_{\mathrm{cl}}^{\mathrm{max}}, \tilde{I}_{\mathrm{cl}}^{\mathrm{ref}}(k)\right)\right), \tag{32c}$$

where $e \in \mathbb{R}$ labels the control error, $T_{\mathrm{cc}}^{\mathrm{ref}} \in \mathbb{R}_{\geq 0}$ the reference temperature, $K_{\mathrm{p}} \in \mathbb{R}$ the controller gain, and $t_{\mathrm{n}} \in \mathbb{R}_{>0}$ the integration time. Clipping (32c) of the theoretically given reference value $\tilde{I}_{\mathrm{cl}}^{\mathrm{ref}}$ (32b) ensures compliance with the current limits (26). Finally, the calculated inputs are applied to the plant.

At the first time step, the initialization according to

$$k = 0, \quad e(-1) = 0, \quad I_{\mathrm{cl}}^{\mathrm{ref}}(-1) = 0, \quad s_{\mathrm{cl/f}}(\text{-}j) = 0 \ \ \forall j > 0 \tag{33}$$

ensures a reliable start-up.

4.2. Observer

Here, an extended Kalman filter [41,44], a state-of-the-art solution for nonlinear model dynamics, is applied. Based on the augmented nonlinear hybrid model (18), it provides estimates of model and disturbance states, $\hat{\boldsymbol{x}}_{\mathrm{c}}$ and $\hat{\boldsymbol{d}}$, in every time step.

During start-up, a set of variables must be initialized. A generally reasonable choice for some of them is given by

$$\hat{\boldsymbol{d}}(\text{-}1) = \boldsymbol{0}, \quad \boldsymbol{u}^{\mathrm{meas}}(\text{-}1) = \boldsymbol{u}^{\mathrm{meas}}(0), \quad \boldsymbol{v}^{\mathrm{meas}}(\text{-}1) = \boldsymbol{v}^{\mathrm{meas}}(0), \tag{34}$$

while plant specifics drive the determination of the remaining ones: the initially estimated model states $\hat{\boldsymbol{x}}_{\mathrm{c}}(\text{-}1)$ and error covariance matrix $\hat{\boldsymbol{P}}(\text{-}1)$. Same holds for filter tuning done by noise variances $\boldsymbol{Q}_{\mathrm{x}}$, $\boldsymbol{Q}_{\mathrm{d}}$, and $\boldsymbol{Q}_{\mathrm{y}}$.

4.3. Hybrid model predictive controller

Hybrid model predictive control means repetitively solving a constrained finite time optimal control problem for a hybrid plant model [20]. Enhancements over the basic HMPC concept allow for fully utilizing the attainable operational flexibility and ensuring real-time capable decision-making. On the one hand, the adaptions to the specific problem involve incorporating the entire system dynamics using the augmented model (24). On the other hand, it covers the design of the objective function and constraints in such a way as to alleviate computational burden while sustaining flexibility and pursuing efficiency aspects and temperature compliance. Both features constitute this work's novel contribution to the optimization aspect of the field. The problem structure of the specific application in this work is schematically depicted in Fig. 5, graphically supporting all upcoming elaborations. Considerations start with the current time step k and

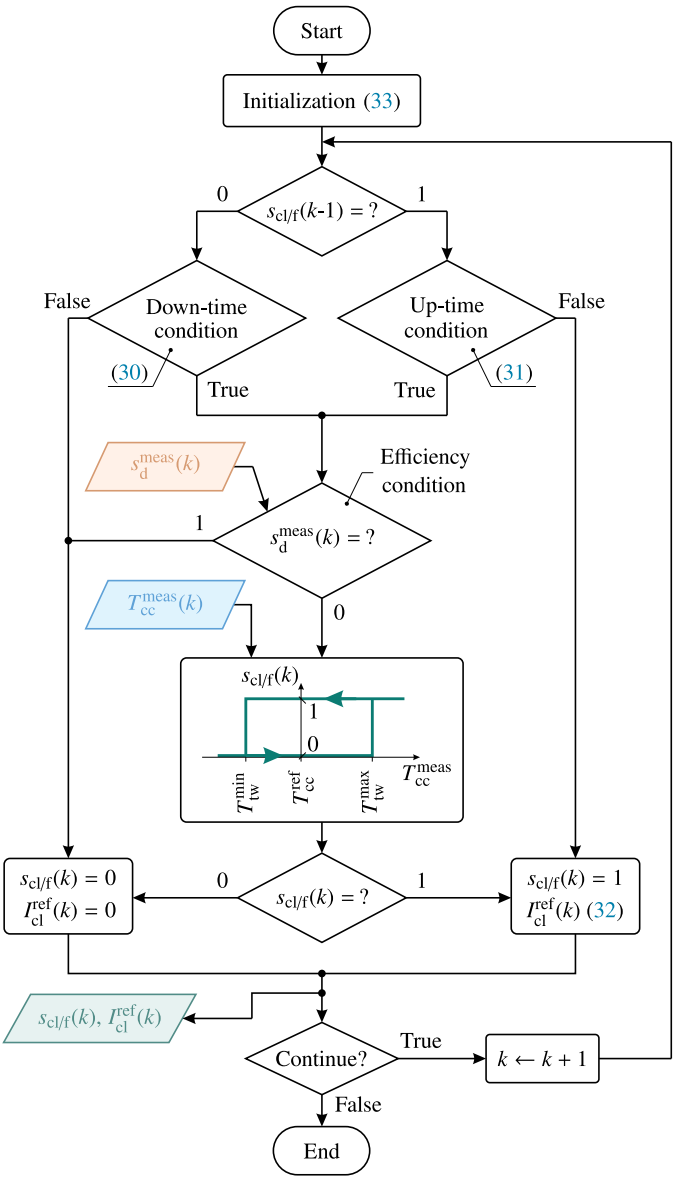

Fig. 4. Flow chart of the rule-based hysteresis proportional–integral control approach, including references to all relevant equations.

include the time evolution of model quantities within a finite horizon. This so-called prediction horizon comprises $N_p \in \mathbb{N}$ future time steps. Changes in the input variables are only allowed within the control horizon comprising $N_c \in \mathbb{N}$ future time steps, for which $N_c \leq N_p$ holds.

4.3.1. Model dynamics

The eventually incorporated switched affine dynamics result from discretizing the augmented affine formulation (24), using the zero-order hold method and sampling time t_s. With the abbreviation $(.) = k+j$, the state and disturbance equations can be written $\forall j \in \{0, 1, \dots, N_p-1\}$ as

$$\begin{aligned} \boldsymbol{x}_c(.+1|k) &= \boldsymbol{A}_d(m,l)\,\boldsymbol{x}_c(.|k) + \boldsymbol{b}_d(m,l)\,u_c(.|k) + \cdots \\ &\quad \boldsymbol{E}_d(m)\,\boldsymbol{v}_c(.|k) + \boldsymbol{g}_d(m,l) \end{aligned} \tag{35a}$$

$$\boldsymbol{d}(.+1|k) = \boldsymbol{d}(.|k), \tag{35b}$$

where $(i|k)$ denotes values at time step i, predicted at time step k, and subscript "d" indicates matrices and vectors related to the discretized

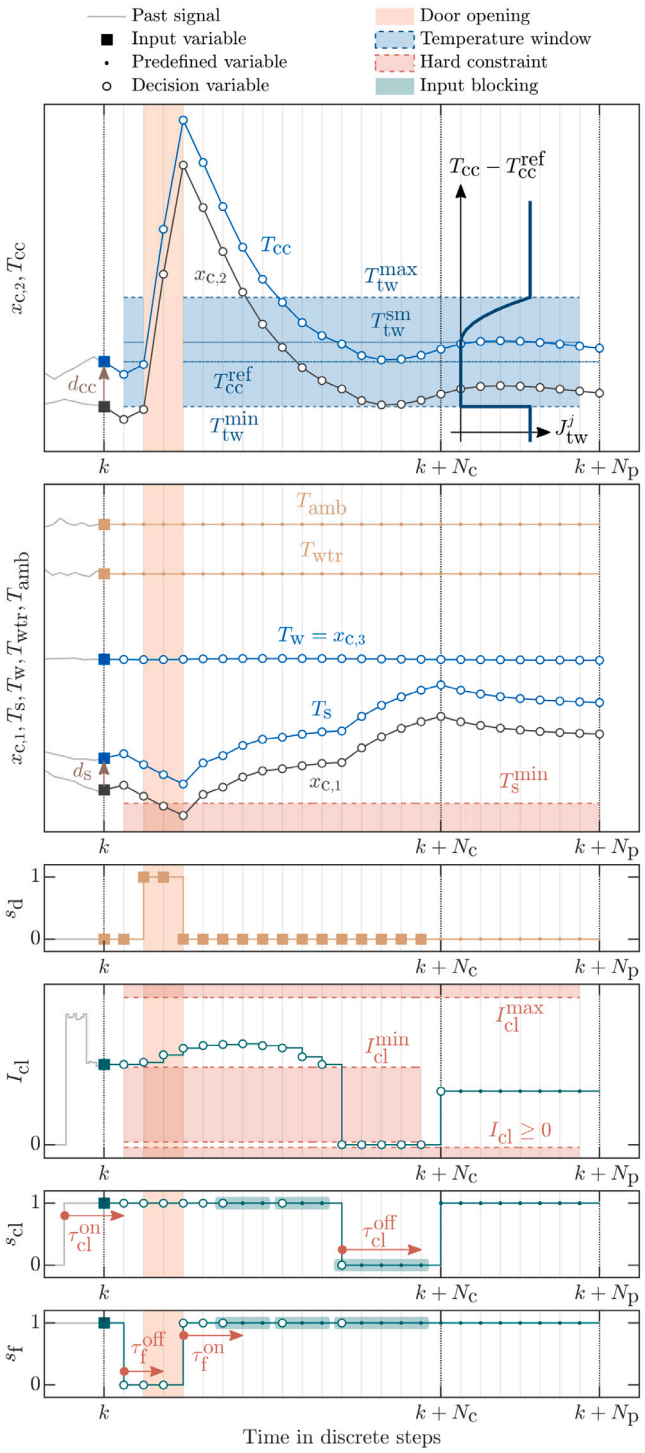

Fig. 5. Exemplary representation of the predictions constituting the hybrid optimal control problem, including all relevant limitations and constraints.

form. The corresponding output equation (24c) evolves to

$$T_{cc}(k+j|k) = x_{c,2}(k+j|k) + d_{cc}(k+j|k) \tag{36a}$$

$$T_s(k+j|k) = x_{c,1}(k+j|k) + d_s(k+j|k), \tag{36b}$$

and the current model mode m results from

$$m = m(.|k) = f_{MS}\left(\boldsymbol{u}_b(.|k), \upsilon_b(.|k)\right). \tag{37}$$

With the affine approach type selected according to

$$l = l(.|k) = \begin{cases} 1 & \dots \ \forall j \in \{0, 1, \dots, N_\mathrm{c}\text{-}1\} \\ 0 & \dots \ \forall j \in \{N_\mathrm{c}, \dots, N_\mathrm{p}\text{-}1\}, \end{cases} \tag{38}$$

this choice ensures high accuracy of the affine approximation in the immediate future, the control horizon. Besides, it comes with an extended validity range for the rest of the prediction horizon. This is necessary since the feasible current range is dilated after the control horizon for computational ease.

4.3.2. Initial conditions

Using capitalized symbols to denote value sets covering the entire horizon, quantities to be determined can be reasonably gathered according to:

$$\boldsymbol{X}_\mathrm{c}(k) = \left[\boldsymbol{x}_\mathrm{c}^\mathrm{T}(k|k),\ \boldsymbol{x}_\mathrm{c}^\mathrm{T}(k{+}1|k),\ \dots,\ \boldsymbol{x}_\mathrm{c}^\mathrm{T}(k{+}N_\mathrm{p}|k)\right]^\mathrm{T} \tag{39a}$$

$$\boldsymbol{D}(k) = \left[\boldsymbol{d}^\mathrm{T}(k|k),\ \boldsymbol{d}^\mathrm{T}(k{+}1|k),\ \dots,\ \boldsymbol{d}^\mathrm{T}(k{+}N_\mathrm{p}|k)\right]^\mathrm{T} \tag{39b}$$

$$\boldsymbol{U}_\mathrm{c}(k) = \left[u_\mathrm{c}(k|k),\ u_\mathrm{c}(k{+}1|k),\ \dots,\ u_\mathrm{c}(k{+}N_\mathrm{p}\text{-}1|k)\right]^\mathrm{T} \tag{39c}$$

$$\boldsymbol{U}_\mathrm{b}(k) = \left[\boldsymbol{u}_\mathrm{b}^\mathrm{T}(k|k),\ \boldsymbol{u}_\mathrm{b}^\mathrm{T}(k{+}1|k),\ \dots,\ \boldsymbol{u}_\mathrm{b}^\mathrm{T}(k{+}N_\mathrm{p}\text{-}1|k)\right]^\mathrm{T} \tag{39d}$$

$$\boldsymbol{V}_\mathrm{c}(k) = \left[\boldsymbol{v}_\mathrm{c}^\mathrm{T}(k|k),\ \boldsymbol{v}_\mathrm{c}^\mathrm{T}(k{+}1|k),\ \dots,\ \boldsymbol{v}_\mathrm{c}^\mathrm{T}(k{+}N_\mathrm{p}\text{-}1|k)\right]^\mathrm{T} \tag{39e}$$

$$\boldsymbol{V}_\mathrm{b}(k) = \left[v_\mathrm{b}(k|k),\ v_\mathrm{b}(k{+}1|k),\ \dots,\ v_\mathrm{b}(k{+}N_\mathrm{p}\text{-}1|k)\right]^\mathrm{T} \tag{39f}$$

Solving an optimal control problem takes a significant part of the sampling time. Therefore, computation results can only be applied reasonably at the beginning of the next time step. This time delay is systematically addressed by assuming the current plant inputs are fixed in the optimization run for the first time step of the horizon. Only the plant inputs beginning with $(k+1)$ are decision variables and free to optimize. Therefore, the current values are the ones provided by the observer or match the measured ones:

$$\boldsymbol{x}_\mathrm{c}(k|k) = \hat{\boldsymbol{x}}_\mathrm{c}(k), \quad \boldsymbol{d}(k|k) = \hat{\boldsymbol{d}}(k) \tag{40a}$$

$$u_\mathrm{c}(k|k) = I_\mathrm{cl}^\mathrm{meas}(k), \quad \boldsymbol{u}_\mathrm{b}(k|k) = \boldsymbol{u}_\mathrm{b}^\mathrm{meas}(k|k) \tag{40b}$$

$$\boldsymbol{v}_\mathrm{c}(k|k) = \boldsymbol{v}_\mathrm{c}^\mathrm{meas}(k), \quad v_\mathrm{b}(k|k) = s_\mathrm{d}^\mathrm{meas}(k) \tag{40c}$$

4.3.3. Control objective

Incorporation of the control objective, textually formulated in Section 4, happens by means of the performance objective $J \in \mathbb{R}_{\geq 0}$ given by

$$J = J_\mathrm{tw} + J_\mathrm{ec} + J_\mathrm{im} + J_\mathrm{tt}. \tag{41}$$

Thereby, $J_\mathrm{tw} \in \mathbb{R}_{\geq 0}$ and $J_\mathrm{ec} \in \mathbb{R}_{\geq 0}$ penalize temperature window violations and energy consumption, respectively. Inefficient modes are considered by $J_\mathrm{im} \in \mathbb{R}_{\geq 0}$, and $J_\mathrm{tt} \in \mathbb{R}_{\geq 0}$ denotes a terminal temperature objective.

Because of the acceptable temperature range, the temperature window objective assigns costs only if limits are violated — see the cost function for a single time step j, J_tw^j, in the top diagram of Fig. 5. Apart from those unsteady costs, an additional term smoothes the function at the upper limit, starting at the smoothing temperature $T_\mathrm{tw}^\mathrm{sm} \in \mathbb{R}_{\geq 0}$. It represents a safety margin to avoid the more severe impact of higher temperatures. Since practical circumstances make it impossible to obey temperature limits during door openings, such periods are excluded. Above elaborations merge into:

$$J_\mathrm{tw} = R_\mathrm{tw} \sum_{j=1}^{N_\mathrm{p}-1} \left[1\text{-}s_\mathrm{d}(k{+}j|k)\right] \left[\delta_\mathrm{tw,b}(k{+}j|k) + S_\mathrm{tw}\delta_\mathrm{tw,c}(k{+}j|k)\right] \tag{42}$$

Here, $R_\mathrm{tw} \in \mathbb{R}_{\geq 0}$ is a weighting factor, and $\delta_\mathrm{tw,b} \in \{0,1\}$ and $\delta_\mathrm{tw,c} \in \{0,1\}$ are the binary and continuous slack variables given as:

$$\delta_\mathrm{tw,b}(.|k) = \begin{cases} 0 & \dots \ T_\mathrm{tw}^\mathrm{min} \leq T_\mathrm{cc}(.|k) \leq T_\mathrm{tw}^\mathrm{max} \\ 1 & \dots \ \text{otherwise} \end{cases} \tag{43a}$$

$$\delta_\mathrm{tw,c}(.|k) = \begin{cases} T_\mathrm{cc}(.|k) - T_\mathrm{tw}^\mathrm{sm} & \dots \ T_\mathrm{tw}^\mathrm{sm} \leq T_\mathrm{cc}(.|k) \leq T_\mathrm{tw}^\mathrm{max} \\ 0 & \dots \ \text{otherwise} \end{cases} \tag{43b}$$

Calculating the smoothing factor $S_\mathrm{tw} \in \mathbb{R}_{\geq 0}$ according to

$$S_\mathrm{tw} = \left(T_\mathrm{tw}^\mathrm{max} - T_\mathrm{tw}^\mathrm{sm}\right)^{-2} \tag{44}$$

ensures a steady transition of the costs at the upper temperature limit. This design approach with joint usage of binary and continuous slack variables corresponds to using solely continuous slack variables with general nonlinear (in particular: binary) mapping into the objective function. Chosen remedy of introducing a binary slack variable favors the performance of the mixed-integer framework.

Integrating the overall energy consumption relies on the model equations for the electrical power, (3) and (10). Extracting the most significant terms yields

$$J_\mathrm{ec} = \left[1 - \omega_\mathrm{pd}(k)\right] \ R_\mathrm{ec} \sum_{j=1}^{N_\mathrm{p}-1} 2\,\alpha_2\, I_\mathrm{cl}^2(k{+}j|k) + \zeta\, s_\mathrm{f}(k{+}j|k) \tag{45}$$

with the weighting factor $R_\mathrm{ec} \in \mathbb{R}_{\geq 0}$ and the pull down switch $\omega_\mathrm{pd} \in \{0,1\}$. This additional input allows neglecting energy consumption entirely, yielding a more temperature-driven control behavior. A generally applicable choice is given as:

$$\omega_\mathrm{pd}(k) = \begin{cases} 0 & \dots \ \hat{T}_\mathrm{cc}(k) \leq T_\mathrm{tw}^\mathrm{max} \\ 1 & \dots \ (k=0) \vee (\text{Reset}) \\ \omega_\mathrm{pd}(k\text{-}1) & \dots \ \text{otherwise} \end{cases} \tag{46}$$

Although ω_pd is only active in this work at start-up and turned off once the upper temperature limit $T_\mathrm{tw}^\mathrm{max}$ is reached, the reset command typifies any application-specific algorithm, indicating the approach's flexibility.

It is highly inefficient to enhance airflow during door openings by activating the fan. Thus, such operating modes are penalized according to

$$J_\mathrm{im} = R_\mathrm{im} \sum_{j=1}^{N_\mathrm{c}-1} s_\mathrm{d}(k{+}j|k)\, s_\mathrm{f}(k{+}j|k), \tag{47}$$

where $R_\mathrm{im} \in \mathbb{R}_{\geq 0}$ is a weighting factor.

The terminal temperature objective effects a steady attraction toward the temperature window and is given as

$$J_\mathrm{tt} = R_\mathrm{tt}^\mathrm{sq}\, \delta_\mathrm{tt}^2(k) + R_\mathrm{tt}^\mathrm{abs}\, \left|\delta_\mathrm{tt}(k)\right|, \tag{48}$$

whereas $R_\mathrm{tt}^\mathrm{sq} \in \mathbb{R}_{\geq 0}$ and $R_\mathrm{tt}^\mathrm{abs} \in \mathbb{R}_{\geq 0}$ label the square and absolute weighting factor, respectively. The slack variable $\delta_\mathrm{tt} \in \{0,1\}$ results from

$$\delta_\mathrm{tt}(k) = T_\mathrm{cc}(k{+}N_\mathrm{p}|k) - T_\mathrm{cc}^\mathrm{ref}. \tag{49}$$

Besides the performance objective, a series of constraints leverage the overall control problem to reasonable computation time and reliable plant operation.

4.3.4. Simplifying constraints

Simplified assumptions for the time steps outside the control horizon realize highly demanded computational alleviation [45]. Firstly, the cooling loop current can only be chosen once within that period, meaning that

$$I_\mathrm{cl}(k{+}j|k) = I_\mathrm{cl}(k{+}N_\mathrm{c}|k), \quad \forall j \in \{N_\mathrm{c}{+}1, \dots, N_\mathrm{p}\text{-}1\} \tag{50}$$

holds. Secondly, the cooling loop and fan are both active in the meanwhile, implemented by

$$\boldsymbol{u}_\mathrm{b}(k{+}j|k) = \mathbf{1}_{2\times 1}, \quad \forall j \in \{N_\mathrm{c}, \dots, N_\mathrm{p}\text{-}1\}. \tag{51}$$

And finally, the condition

$$s_{\mathrm{d}}(k+j|k) = 0, \quad \forall j \in \{N_{\mathrm{c}}, \dots, N_{\mathrm{p}}\text{-}1\} \tag{52}$$

is assumed true. Although these simplifications appear restrictive, they are essential for a real-time operation and only slightly influence the immediate control action as they are only predicted and never implemented in the eventual receding horizon control law.

4.3.5. Technological constraints

Back to general limitations, the storage temperature must obey a minimum value $T_{\mathrm{s}}^{\min} \in \mathbb{R}_{\geq 0}$ due to technological constraints:

$$T_{\mathrm{s}}(k+j|k) \geq T_{\mathrm{s}}^{\min}, \quad \forall j \in \{1, 2, \dots, N_{\mathrm{p}}\} \tag{53}$$

Considering manipulated continuous inputs, the cooling loop current must comply with minimum and maximum limits, as mentioned in (26). In the predictive scheme, it is implemented $\forall j \in \{1, 2, \dots, N_{\mathrm{c}}\text{-}1\}$ as

$$s_{\mathrm{cl}}(k+j|k)\, I_{\mathrm{cl}}^{\min} \leq I_{\mathrm{cl}}(k+j|k) \leq s_{\mathrm{cl}}(k+j|k)\, I_{\mathrm{cl}}^{\max}. \tag{54}$$

However, the lower limit is omitted outside the prediction horizon due to the above-mentioned simplified assumptions therein, yielding

$$0 \leq I_{\mathrm{cl}}(k+j|k) \leq I_{\mathrm{cl}}^{\max}, \quad \forall j \in \{N_{\mathrm{c}}, \dots, N_{\mathrm{p}}\text{-}1\}. \tag{55}$$

4.3.6. Minimum up- and down-times

Minimum up- and down-times of the cooling loop and fan, demanded by (27), are incorporated into the optimal control problem using a similar formulation as presented in [46]:

$$s_{\{\mathrm{cl,\ f}\}}(k+j|k) - s_{\{\mathrm{cl,\ f}\}}(k+j\text{-}1|k) \leq s_{\{\mathrm{cl,\ f}\}}(k+i|k) \tag{56a}$$

$$s_{\{\mathrm{cl,\ f}\}}(k+j\text{-}1|k) - s_{\{\mathrm{cl,\ f}\}}(k+j|k) \leq 1 - s_{\{\mathrm{cl,\ f}\}}(k+i|k) \tag{56b}$$

$$\forall j \in \left\{ \text{-}N_{\{\mathrm{cl,\ f}\}}^{\{\mathrm{on,\ off}\}}\text{+}1, \dots, N_{\mathrm{c}}\text{-}N_{\{\mathrm{cl,\ f}\}}^{\{\mathrm{on,\ off}\}} \right\} \tag{56c}$$

$$\forall i \in \left\{ j\text{+}1, j\text{+}2, \dots, j\text{+}N_{\{\mathrm{cl,\ f}\}}^{\{\mathrm{on,\ off}\}}\text{-}1 \right\} \tag{56d}$$

Therefore, necessary preceding switching states are either available through logged measurements or assumed to be 0 before the initial start-up at $k = 0$. Thus, the relation

$$s_{\{\mathrm{cl,\ f}\}}(k+r|k) = \begin{cases} s_{\{\mathrm{cl,\ f}\}}^{\mathrm{meas}}(k+r) & \dots\ k+r > 0 \\ 0 & \dots\ \text{otherwise} \end{cases} \tag{57}$$

holds $\forall r \in \mathbb{Z}_{<0}$.

4.3.7. Move blocking

Since binary variables drastically increase problem complexity, implementation of move blocking [47], more precise input blocking, further alleviates the computational burden. Thus, the binary inputs can only be freely chosen on a reduced number of time steps, $N_{\mathrm{mb}} \in \mathbb{N}$, $N_{\mathrm{mb}} \leq N_{\mathrm{c}}\text{-}1$, within the control horizon — see the markings in the two bottom diagrams of Fig. 5. The reduced binary decision vector $\boldsymbol{U}_{\mathrm{b}}^{\mathrm{red}} \in \{0,1\}^{2\,N_{\mathrm{mb}}}$, given by

$$\boldsymbol{U}_{\mathrm{b}}^{\mathrm{red}}(k) = \left[\boldsymbol{u}_{\mathrm{b},1}^{\mathrm{red^T}}(k),\ \boldsymbol{u}_{\mathrm{b},2}^{\mathrm{red^T}}(k),\ \dots,\ \boldsymbol{u}_{\mathrm{b},N_{\mathrm{mb}}}^{\mathrm{red^T}}(k) \right]^{\mathrm{T}}, \tag{58}$$

can be transformed back into its comprehensive counterpart by

$$\boldsymbol{U}_{\mathrm{b}}(k\text{+}1 \rightarrow k\text{+}N_{\mathrm{c}}\text{-}1|k) = \left(\boldsymbol{T}_{\mathrm{mb}} \otimes \boldsymbol{I}_2 \right) \boldsymbol{U}_{\mathrm{b}}^{\mathrm{red}}(k). \tag{59}$$

Here, $\otimes$ is the Kronecker product, and $\boldsymbol{I}_2$ denotes an identity matrix of size 2×2. With slight abuse of notation, the sparse move-blocking matrix $\boldsymbol{T}_{\mathrm{mb}} \in \{0,1\}^{N_{\mathrm{c}}\text{-}1 \times N_{\mathrm{mb}}}$ can be written as

$$\boldsymbol{T}_{\mathrm{mb}}(r,c) = \begin{cases} 1 & \dots\ (r,c) = \left(\boldsymbol{r}_{\mathrm{mb}}(i), \boldsymbol{c}_{\mathrm{mb}}(i) \right), \forall i \\ 0 & \dots\ \text{otherwise}, \end{cases} \tag{60}$$

meaning that the matrix entries are only of value 1 if the row-column pair (r,c) is contained in the set formed by the associated vectors $\boldsymbol{r}_{\mathrm{mb}}$ and $\boldsymbol{c}_{\mathrm{mb}}$, and otherwise 0.

4.3.8. Disturbance predictions

Lastly, the optimal control problem needs forecasts for the disturbance inputs. Since the ambient and water temperature are just subject to slight changes, a zero-order prediction model proves suitable, yielding

$$\boldsymbol{v}_{\mathrm{c}}(k+j|k) = \boldsymbol{v}_{\mathrm{c}}(k|k), \quad \forall j \in \{1, 2, \dots, N_{\mathrm{p}}\text{-}1\}. \tag{61}$$

Regarding future door openings, the control scheme utilizes the externally provided expected door opening trajectory $s_{\mathrm{d}}^{\mathrm{exp}}$ if it matches the measured one at the current time step. Otherwise, an approximate guess will be made. Thus, the relation

$$s_{\mathrm{d}}(k+j|k) = \begin{cases} s_{\mathrm{d}}^{\mathrm{exp}}(k+j|k) & \dots\ s_{\mathrm{d}}^{\mathrm{exp}}(k|k) = s_{\mathrm{d}}^{\mathrm{meas}}(k|k) \\ \text{Guess} & \dots\ \text{otherwise} \end{cases} \tag{62}$$

holds $\forall j \in \{1, 2, \dots, N_{\mathrm{c}}\text{-}1\}$. In detail, this work assumes an open door for another period $t_{\mathrm{d}}^{\mathrm{unexp}} \in \mathbb{R}_{\geq 0}$ if an unexpected event occurs. However, guesses can be adapted flexibly to account for specific circumstances.

4.3.9. Control law

Finally, the optimal input sequences, indicated by a superscript asterisk, result from solving the overall mixed-integer control problem given as

$$\left[\boldsymbol{U}_{\mathrm{c}}^{*}(k), \boldsymbol{U}_{\mathrm{b}}^{\mathrm{red}*}(k) \right] = \underset{\left[\boldsymbol{U}_{\mathrm{c}}(k), \boldsymbol{U}_{\mathrm{b}}^{\mathrm{red}}(k) \right]}{\arg\min} \ J \tag{63}$$

subject to:

- Model dynamics (35)–(38)
- Initial conditions (40)
- Simplifying constraints (50)–(52)
- Technological constraints (53)–(55)
- Minimum up- and down-times (56),(57)
- Move blocking (58)–(60)
- Disturbance predictions (61),(62)

The control algorithm is implemented in MATLAB [48], whereas the optimization problem is built using YALMIP [49] and solved by Gurobi optimizer [50]. An optimizer time limit of 90% of the sampling time ensures that at least a suboptimal solution can be processed at every time step. Hence, the control input

$$\boldsymbol{u}^{\mathrm{ref}}(k\text{+}1) = \left[u_{\mathrm{c}}^{*}(k\text{+}1|k),\ \boldsymbol{u}_{\mathrm{b}}^{*\mathrm{T}}(k\text{+}1|k) \right]^{\mathrm{T}} \tag{64}$$

will be applied to the plant at the beginning of the next time step, $k \leftarrow k\text{+}1$. This procedure is then reiterated, rendering it a receding horizon control scheme.

4.4. Model predictive controller

The high computational burden of HMPC approaches often limits their practical applicability [45]. Therefore, industrial applications favor ordinary predictive approaches. Such a scheme is deduced from the flexible HMPC formulation (63) by imposing further limitations. These comprise two substantial simplifications:

Firstly, the cooling loop and fan can only operate together. Implemented as

$$s_{\mathrm{cl}}(k+j|k) = s_{\mathrm{f}}(k+j|k), \quad \forall j \in \left\{1, 2, \dots, N_{\mathrm{c}}\text{-}1\right\}, \tag{65}$$

it eliminates any flexibility provided by the thermal storage.

Secondly, the door opening is now incorporated using an additional continuous model input, the door heat flow $\dot{Q}_{\mathrm{d}} \in \mathbb{R}$. Thus, the vector of continuous disturbances extends as

$$\boldsymbol{v}_{\mathrm{c}}(t) \leftarrow \boldsymbol{v}_{\mathrm{c}}^{\mathrm{MPC}}(t) = \left[T_{\mathrm{amb}}(t),\ T_{\mathrm{wtr}}(t),\ \dot{Q}_{\mathrm{d}}(t) \right]^{\mathrm{T}}, \tag{66}$$

motivating the substitution of (7) according to

$$\dot{Q}_{\mathrm{amb}}(t) \leftarrow \dot{Q}^{\mathrm{MPC}}_{\mathrm{amb}}(t) = \xi_1 \left[T_{\mathrm{amb}}(t) - T_{\mathrm{cc}}(t)\right] + \dot{Q}_{\mathrm{d}}(t). \tag{67}$$

These adaptions further entail modifications of the model dynamics (35) according to

$$\boldsymbol{A}_{\mathrm{d}}(m,l) \leftarrow \boldsymbol{A}^{\mathrm{MPC}}_{\mathrm{d}}(m,l), \quad \boldsymbol{E}_{\mathrm{d}}(m) \leftarrow \boldsymbol{E}^{\mathrm{MPC}}_{\mathrm{d}}(m), \tag{68}$$

where the corresponding superscript highlights quantities related to the MPC approach.

The above simplifications raise the need for a suitable prediction model for $\dot{Q}_{\mathrm{d}}$. For finding such, the model Eqs. (5)–(10) serve as starting point. A sensible assumption is that the fan is off if the door is open. Due to (65), the cooling loop is then turned off as well. This yields the basic prediction model according to

$$\begin{aligned} \chi\, \dot{T}^{\mathrm{Q}}_{\mathrm{cc}}(t) \quad &= \left(-\gamma_2 - \kappa_2 - \xi_1 - \xi_2\right) T^{\mathrm{Q}}_{\mathrm{cc}}(t) + \cdots \\ &\quad \gamma_2\, T_{\mathrm{s}}(t) + \kappa_2\, T_{\mathrm{w}}(t) + \left(\xi_1 + \xi_2\right) T_{\mathrm{amb}}(t) \end{aligned} \tag{69a}$$

$$\dot{Q}_{\mathrm{d}}(t) = \xi_2 \left[T_{\mathrm{amb}}(t) - T^{\mathrm{Q}}_{\mathrm{cc}}(t)\right], \tag{69b}$$

where a superscript "Q" indicates quantities differently calculated to the comprehensive model. With the further assumption that T_{s}, T_{w}, and T_{amb} are constant within the entire horizon, the discrete-time prediction model follows $\forall j \in \{0, 1, \ldots, N_{\mathrm{p}}-1\}$ according to

$$T^{\mathrm{Q}}_{\mathrm{cc}}(.+1|k) = \begin{cases} a^{\mathrm{Q}}_{\mathrm{d}}\, T^{\mathrm{Q}}_{\mathrm{cc}}(.|k) + \boldsymbol{b}^{\mathrm{Q}^{\mathrm{T}}}_{\mathrm{d}} \boldsymbol{u}^{\mathrm{Q}}(k) & \ldots\ s_{\mathrm{d}}(.|k) = 1 \\ T^{\mathrm{Q}}_{\mathrm{cc}}(k|k) & \ldots\ s_{\mathrm{d}}(.|k) = 0 \end{cases} \tag{70a}$$

$$T^{\mathrm{Q}}_{\mathrm{cc}}(k|k) = \hat{x}_{\mathrm{c},2}(k) + \hat{d}_{\mathrm{cc}}(k) \tag{70b}$$

$$\dot{Q}_{\mathrm{d}}(.|k) = s_{\mathrm{d}}(.|k)\, \xi_2 \left[T^{\mathrm{meas}}_{\mathrm{amb}}(k) - T^{\mathrm{Q}}_{\mathrm{cc}}(.|k)\right] \tag{70c}$$

with the abbreviation $(.) = (k+j)$, the eigenvalue $a^{\mathrm{Q}}_{\mathrm{d}} \in \mathbb{R}$, and the input vector $\boldsymbol{b}^{\mathrm{Q}}_{\mathrm{d}} \in \mathbb{R}^3$. Besides, the vector of all prediction model inputs, $\boldsymbol{u}^{\mathrm{Q}} \in \mathbb{R}^3$, is given by

$$\boldsymbol{u}^{\mathrm{Q}}(k) = \left[\hat{x}_{\mathrm{c},1}(k) + \hat{d}_{\mathrm{s}}(k),\ \hat{x}_{\mathrm{c},3}(k),\ T^{\mathrm{meas}}_{\mathrm{amb}}(k)\right]^{\mathrm{T}}. \tag{71}$$

This approach can handle several door openings within the horizon by resetting the modeled cooling chamber temperature after each event (70a).

In summary, the MPC scheme solves a severely restricted form of the HMPC control problem (63) by imposing the additional simplifications (65)–(68), (70), and (71). Applying the control input to the plant remains unaltered to the HMPC case.

5. Experimental setup

Following the original system, the experimentally investigated test bed is geometrically similar, sufficiently insulated, and equipped with various sensors allowing in-depth evaluations, see Fig. 6. Specifically, the sensor position shown in Fig. 6 c ensures measuring a temperature being characteristic of the entire cooling chamber. That was found by [37] and confirmed by preliminary studies. The setup uses two identical cooling units (Figs. 6 d,e) to provide a reasonable total cooling power. As they are operated in parallel, they act together like one more powerful unit, precisely as considered within the control schemes.

Regarding data acquisition and processing, an input/output board communicates with sensors, transducers, and actuators on the field level — see Fig. 7 for an overview and Appendix A for component details. While the intended fan switch is directly applied to the plant, a subjacent control structure handles the operation of Peltier elements. Therefore, a standard approach comprising a buck converter [51] and a simple current controller [52] realizes the given reference. A thorough description of the subjacent control structure applied on this very test bed can be found in [21]. During regular operation, Peltier elements are limited to 85% of their theoretical current limit to, on the one hand, increase lifetime and, on the other hand, inhibit significant thermal noise at high current values [53].

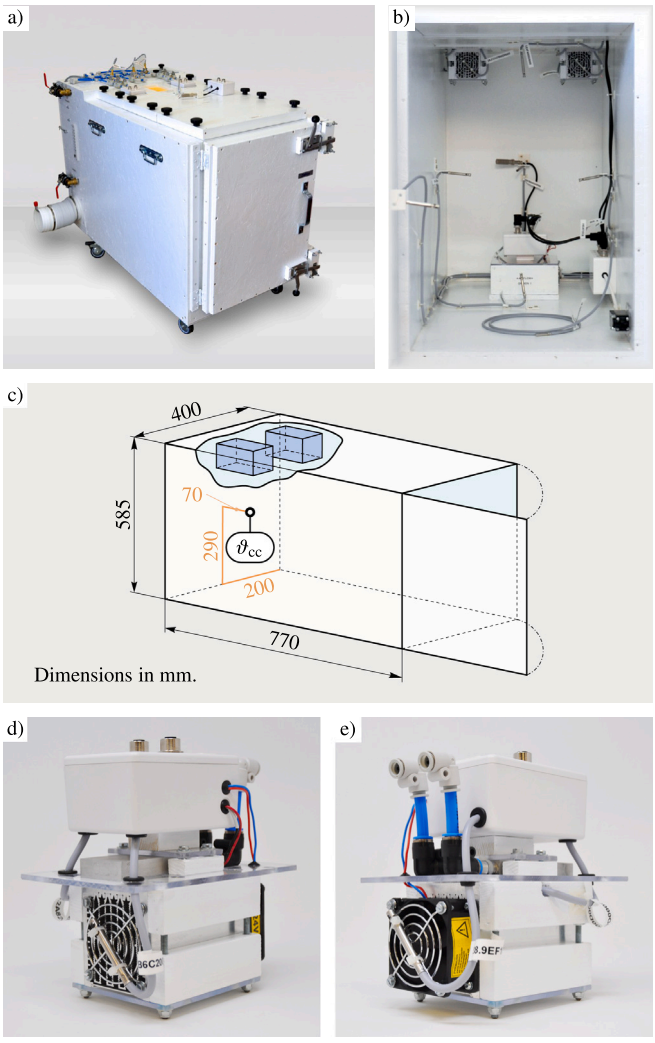

Fig. 6. Experimentally evaluated test bed in (a) exterior and (b) interior view with (c) its dimensions and positioning of the sensor measuring the temperature of the air inside the cooling chamber, ϑ_{cc}. Subfigures (d) and (e) depict a single cooling unit in front and rear view, respectively.

While the computationally simple control schemes, PI and MPC, get along with a local computation unit's capacity, HMPC optimizations are challenging and, therefore, run on a computation server connected via a virtual private network.

6. Results

6.1. Experimental procedure

Experimental investigations using the presented setup (Section 5) serve model parameterization and control performance assessment.

Open-loop experiments provide appropriate data for model training and validation. Thereby, the system input sequences are chosen in such a manner as to grasp all operating modes and to cover the input, state, and output range in a way representative of the eventual application.

Evaluation of control performance relies on closed-loop operation controlled by the PI, MPC, and HMPC scheme. Each control test run $\mathcal{S}$ consists of five scenarios:

$$\mathcal{S} = \left\{S_1, S_2, S_3, S_4, S_5\right\} \tag{72}$$

Scenarios S_1, S_2, and S_3 deal with expected door openings, i.e., both predictive approaches anticipate upcoming door openings. S_1 includes

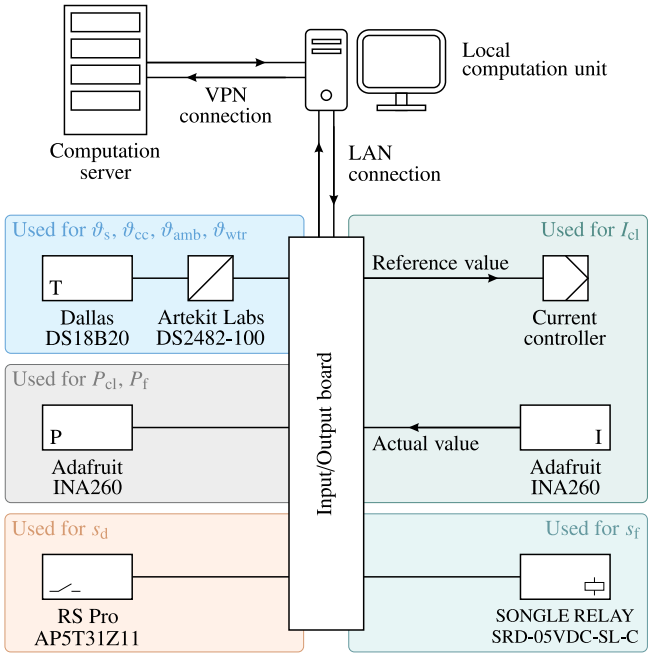

Fig. 7. Data acquisition and processing architecture comprising essential sensors, transducers, actuators, and computation units — see Appendix A for component details. Computation units communicate via a local area network (LAN) or virtual private network (VPN). Symbols according to DIN 19227-2 [54].

a 3-minute, $\mathcal{S}_2$ a 2-minute followed by another 2-minute shortly afterwards, and $\mathcal{S}_3$ a 5-minute door opening. In contrast, the 2-minute door opening in Scenario $\mathcal{S}_4$ occurs unexpectedly. Finally, $\mathcal{S}_5$ considers the pull-down operation starting from a steady state induced by ambient conditions. Besides, every scenario includes periods when the cooling chamber temperature remains within its intended limits. They are sufficiently long to inclusively assess the associated limit-cycle operation. Within a test run, all scenarios were run through immediately one after the other. Although the actual run started with $\mathcal{S}_5$, followed by $\mathcal{S}_1$-$\mathcal{S}_4$, they are rearranged for explanatory reasons.

Special care was taken to ensure the same environmental conditions for all controller test runs, see Fig. 8. Water temperature variations during $\mathcal{S}_5$ arose from slightly unsteady start-up conditions of the fresh water cooling but are sufficiently small to have negligible influence.

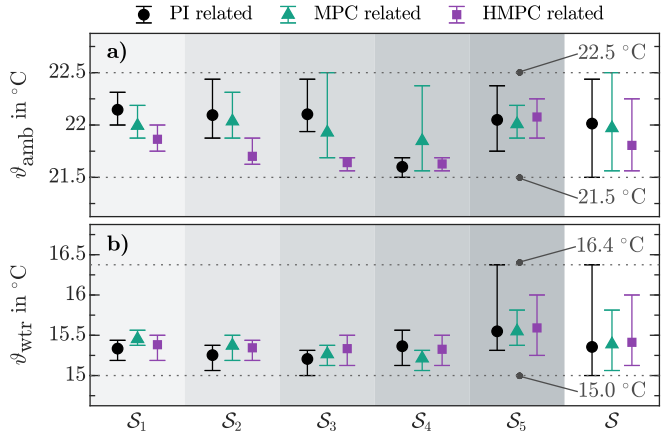

Fig. 8. Environmental conditions (ambient temperature ϑ_{amb} and water temperature ϑ_{wtr}) during control test runs, examined globally for the entire run $\mathcal{S}$ and split up into its single sequences $\mathcal{S}_i$, $i \in \{1, 2, \ldots, 5\}$.

6.2. Model performance

With experimentally captured training data sets, applying methods described in Section 3.4 yields a suitable parameterization for the hybrid model (15),(17). Its high performance becomes evident when evaluated on validation data, see Fig. 9. Although reduced in order compared with the original system's model [19], it achieves similar fitting values. This verifies the systems' dynamic equivalence and the model's broad applicability to differently sized systems.

Numerical values of estimated model parameters (14) and coefficients of the affine approach (23) are provided in Appendix B.

6.3. Controller tuning

PI parameters, i.e., controller gain K_p and integration time t_n, have been determined based on an experimentally captured step response

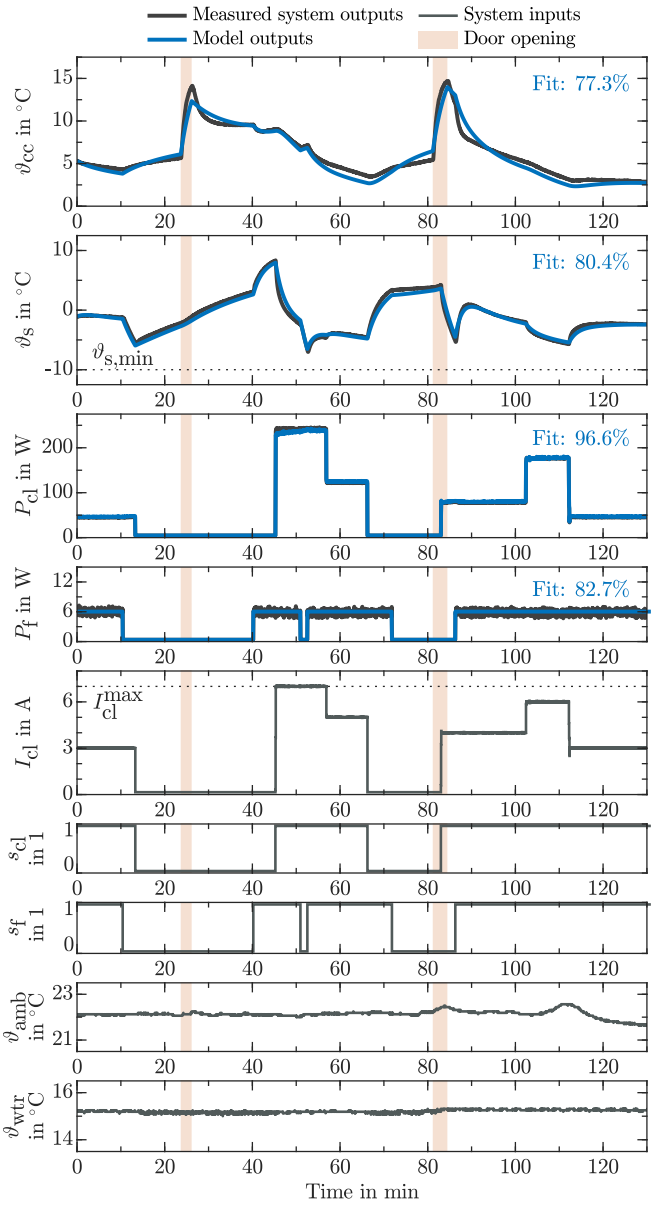

Fig. 9. Experimentally applied system inputs and comparison of measured system outputs and model outputs, based on validation data. Indicated model fit is calculated as given in [19].

and applying the Chien-Hrones-Reswick method [55] for 0% overshoot and disturbance rejection.

The basic parameters (sampling time t_s, horizon lengths N_p and N_c) obey standard guidelines [56], enabling a closed-loop performance sufficiently close to global optimality. Applying the Nyquist theorem on the door opening dynamics, i.e., the fastest system dynamics, dictates an upper limit for t_s. A lower limit for N_p results from the slowest system dynamics. As the optimal control problem includes a terminal objective (48), it is equivalent to an infinite horizon control problem [56] and, therefore, fulfills this demand implicitly. According to [57,58], the input flexibility at the beginning of the horizon determines the obtainable closed-loop optimality and its effect stagnates above a certain problem-specific threshold. Comprehensive closed-loop simulations were used to search for a combination of N_c, move blocking (Section 4.3.7), and simplifying constraints (Section 4.3.4) that lowers complexity but maintains closed-loop optimality.

The remaining objective weights influence the trade-off between temperature compliance and energy consumption but do not affect optimality. They are chosen to gain the same temperature performance with the HMPC as with the PI scheme for expected door openings. MPC and HMPC are weighted identically to highlight the mutual influence of reduced flexibility on temperature compliance and energy consumption. This parameterization (see Appendix C for numerical values) was chosen to facilitate an at-first-glance comparison of the controllers.

6.4. Control performance

The experimental procedure described in Section 6.1 drives the performance assessment of all introduced controllers. Numerical evaluation of any control scheme $ctr \in \{\text{PI, MPC, HMPC}\}$ relies upon energy consumption and temperature violation metrics for every scenario $\mathcal{S}_i$, $i \in \{1, 2, \dots, 5\}$ and the overall test run $\mathcal{S}$, see time series data in Figs. 10 and 11. Energy-related assessment (73) comprises the absolute energy consumption $E_{cu} \in \mathbb{R}_{\geq 0}$, the mean total energy consumption $\bar{E}_{cu}^{tot} \in \mathbb{R}_{\geq 0}$, the relative energy consumption to the PI approach, $\Delta E_{cu} \in \mathbb{R}$, and the associated total value $\Delta E_{cu}^{tot} \in \mathbb{R}$. Thereby, $n_k \in \mathbb{N}$ denotes the total number of time steps within the considered data set.

$$E_{cu}(k; ctr) = t_s \sum_{j=0}^{k-1} P_{cl}(j; ctr) + P_f(j; ctr) \tag{73a}$$

$$\bar{E}_{cu}^{tot}(ctr) = E_{cu}(n_k; ctr) / \left(t_s\, n_k\right) \tag{73b}$$

$$\Delta E_{cu}(k; ctr) = \left[E_{cu}(k; ctr) - E_{cu}(k; \text{PI})\right] / E_{cu}(n_k; \text{PI}) \tag{73c}$$

$$\Delta E_{cu}^{tot}(ctr) = \Delta E_{cu}(n_k; ctr) \tag{73d}$$

According to the temperature performance objective (42), temperature violations are only considered in periods of a closed door. Related metrics (74) are the cumulated temperature violation $V_\vartheta \in \mathbb{R}_{\geq 0}$, the associated total average $\bar{V}_\vartheta \in \mathbb{R}_{\geq 0}$, and the relative difference in temperature violation to the PI approach, $\Delta V_\vartheta \in \mathbb{R}$.

$$\begin{aligned} V_\vartheta(k; ctr) \quad = \sum_{j=0}^{k-1} s_d(j) \max\left(0, T_{cc}(j; ctr) - T_{tw}^{max}\right) + \cdots \\ s_d(j) \max\left(0, T_{tw}^{min} - T_{cc}(j; ctr)\right) \end{aligned} \tag{74a}$$

$$\bar{V}_\vartheta(ctr) = V_\vartheta(n_k; ctr) / n_k \tag{74b}$$

$$\Delta V_\vartheta(ctr) = \left[V_\vartheta(n_k; ctr) - V_\vartheta(n_k; \text{PI})\right] / V_\vartheta(n_k; \text{PI}) \tag{74c}$$

6.4.1. Expected door openings

In handling expected door openings, i.e., in scenarios $\mathcal{S}_1$-$\mathcal{S}_3$, MPC and HMPC fully benefit from their predictive nature (Fig. 10). However, only the HMPC, with its independent actuation of the cooling loop and fan, can harness the flexibility provided by the thermal storage. Separately charging increases the temperature difference to the air inside the chamber and, therefore, the immediate cooling capacity. The HMPC achieves the fastest initial cooldown after a door event — see top diagram in Fig. 10. Besides, this flexibility shortens high ϑ_{cc} values after a door opening. Proper fan operation causes alternating charging and rapid discharging, accelerating cooldown. Another benefit appears between the two door openings in $\mathcal{S}_2$. Since the second door event would render further air cooling holistically inefficient, the HMPC turns off the fan to charge the storage. This allows intensified cooling when energetically reasonable, i.e., after the door closes.

Regarding the operation within the temperature window, its bounds directly dictate the limit cycle of the storage and cooling chamber temperature in the PI case. Contrary, both predictive schemes maintain safety margins, yielding shorter limit cycles of ϑ_{cc}. While it is tied to the limit cycle of ϑ_s in the MPC case, the HMPC broadly exploits the permitted storage temperature, entailing a longer limit cycle.

Since the PI approach solely acts upon temperature-related issues, inefficient operating conditions are not avoided causing significantly higher energy demand — see the power and energy comparisons in Fig. 10. The longer the door openings, the higher the potential energy savings due to predictive approaches (bottom diagram in Fig. 10). Although their energy performances converge with increased total door opening length, the HMPC outperforms the MPC in terms of temperature violation — see the numerical comparison in Fig. 12.

Compared with the PI approach, this also holds, except for scenario $\mathcal{S}_2$. There, the decline in temperature performance results from the anticipatory storage charging described above.

6.4.2. Unexpected door openings

Unexpectedly occurring door openings (scenario $\mathcal{S}_4$ in Fig. 11 a) render the predictive aspect of MPC and HMPC slightly less beneficial. However, attained energy savings are still significant but lower than when door openings were known upfront. Again, the HMPC's optimal storage management improves temperature compliance (Fig. 12).

6.4.3. Pull-down operation

When evaluating the pull-down operation (Fig. 11 b), slight variations in the initial conditions compromise the comparison. As a remedy, all measurements are synchronized in time at the moment when the cooling chamber temperature reaches the upper limit. Furthermore, only the period after the last controller activates the cooling loop is evaluated (energy synchronization). These measures exclude the time and energy taken to obtain the same initial conditions from further consideration. Since all controllers operate at full power until the upper temperature limit, temperature performances are identical and, thus, excluded from Fig. 12 b. Nonetheless, once inside the temperature window, both predictive approaches operate efficiency-focused due to the energy consumption objective (45). This implies a trajectory alongside the upper limit, yielding slight energy savings compared with the PI case.

7. Discussion

All in all, the HMPC approach shows highly satisfactory performance (Fig. 12). This also holds when compared with energy savings others achieved on thermal plants by control strategies [26,35,59], hardware adaptions [42,60,61], and their combinations [24,32]. Therefore, HMPC proves suitable to simultaneously reduce energy costs and loss of goods due to temperature violations in mobile refrigeration applications.

During operation within the temperature window, the energy consumption remains independent of the applied control strategy — see bottom diagrams in Figs. 10 and 11. If the setup possessed a distinctive efficiency peak at an input current higher than the minimum, MPC and HMPC could improve efficiency.

The versatile HMPC structure allows easy adaption to different system scales and architectures. Thus, its application in larger cooling

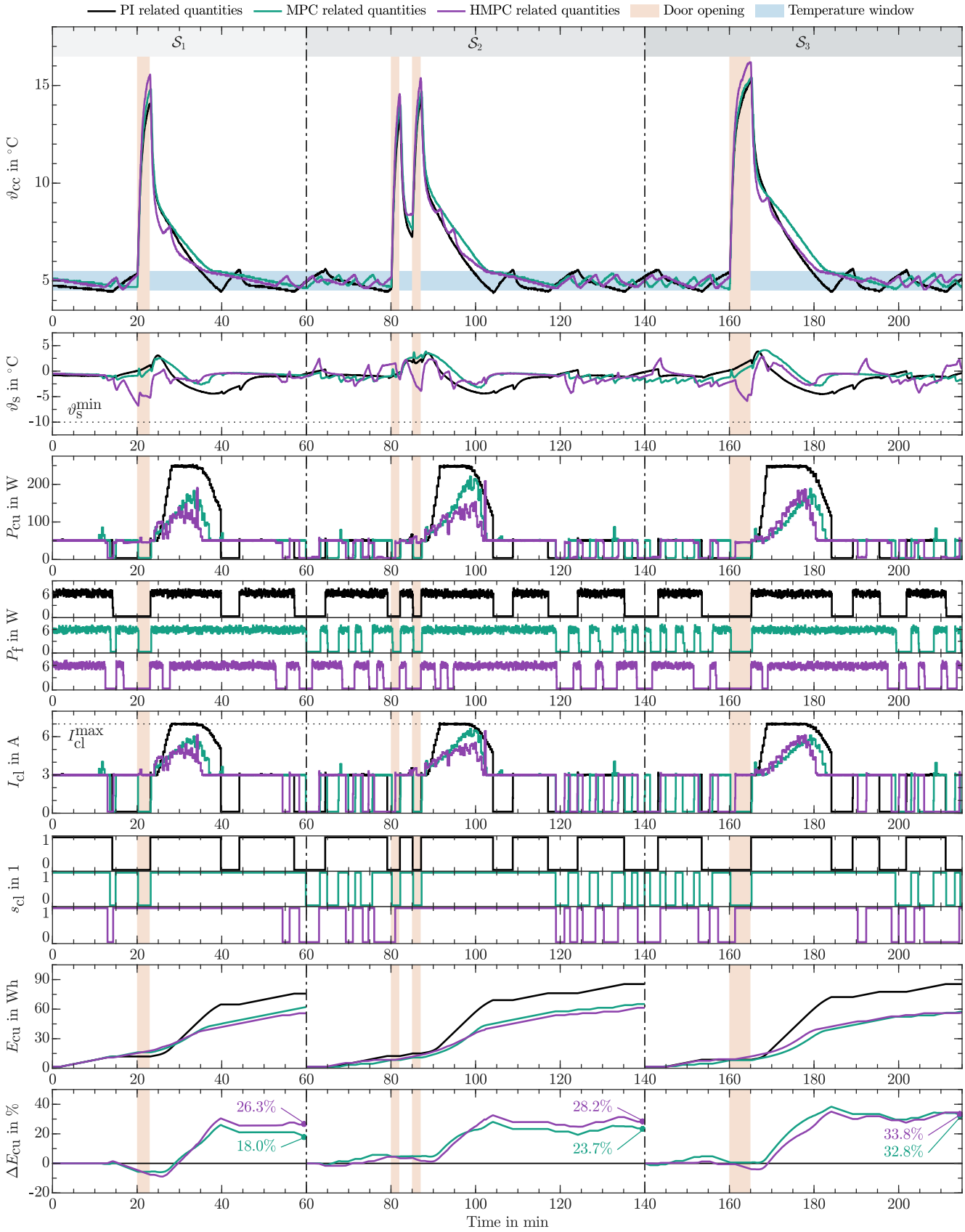

Fig. 10. Time-domain comparison of closed-loop results obtained for scenarios with expected door openings ($\mathcal{S}_1$, $\mathcal{S}_2$, and $\mathcal{S}_3$). The two upper diagrams depict temperature quantities, and the following two relate to electrical power consumption. While the control inputs of the cooling loop are presented in the two subsequent ones, the fan switch s_f is indirectly given by the fan power P_f ($s_f = 1 \Leftrightarrow P_f > 0$). Energy-related performance metrics (73) are given in the lower two diagrams, separately evaluated for each scenario.

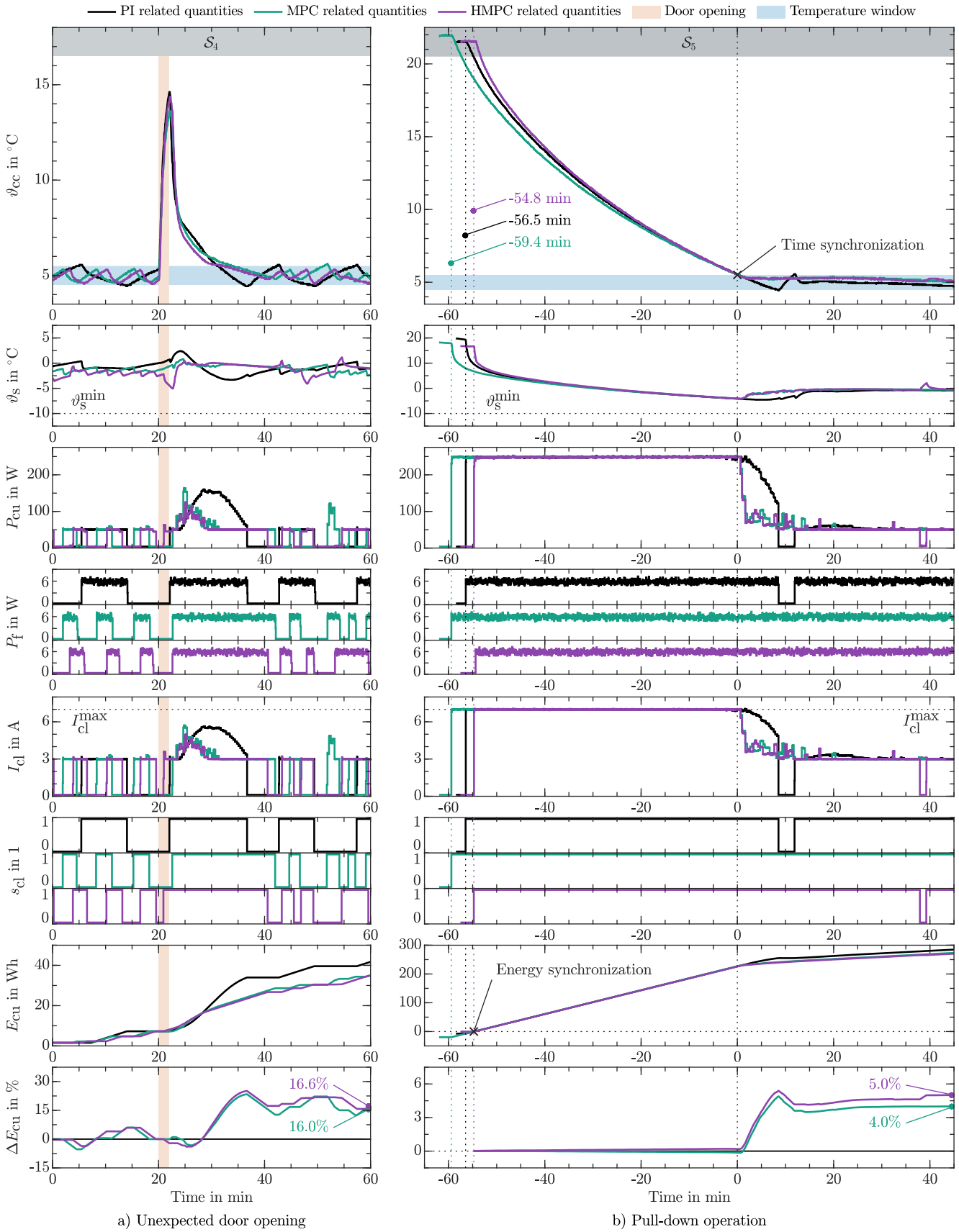

Fig. 11. Time-domain comparison of closed-loop results obtained for (a) an unexpected door opening ($\mathcal{S}_4$) and (b) pull-down operation ($\mathcal{S}_5$). The two upper diagrams depict temperature quantities, and the following two relate to electrical power consumption. While the control inputs of the cooling loop are presented in the two subsequent ones, the fan switch s_f is indirectly given by the fan power P_f ($s_f = 1 \Leftrightarrow P_f > 0$). Energy-related performance metrics (73) are given in the lower two diagrams.

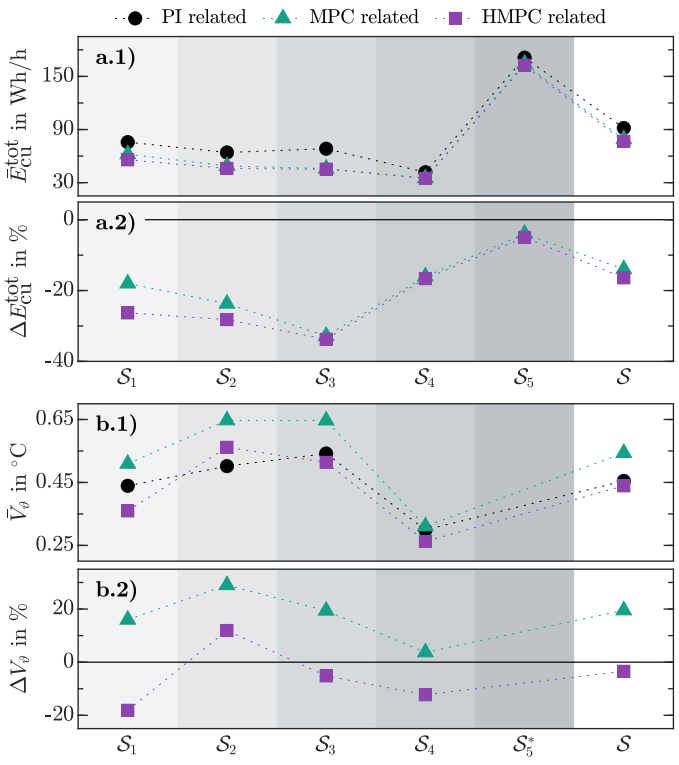

Fig. 12. Control performance values related to (a) energy consumption (73) and (b) temperature violation (74) calculated for each scenario $\mathcal{S}_i$, $i \in \{1, 2, \dots, 5\}$ and the entire test run $\mathcal{S}$.
* Temperature performance is not comparable for pull-down operation.

trucks with several temperature zones seems promising and straightforward. Besides, further efficiency potential would arise if the transportation were restricted to a specific cargo with well-known thermal properties. Then, the model can be extended by cargo temperature estimations [62] to control the goods' temperature directly.

However, HMPC's flexibility comes at the expense of computational complexity, see Fig. 13. As a result, expensive optimization tasks are only solved suboptimally, terminated by the time limit of 18 s. Although computed on a less powerful unit, the MPC approach always yields optimal results but only performs on a level between PI and HMPC due

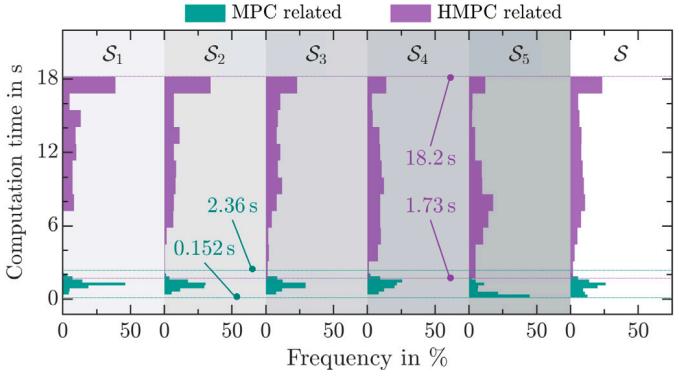

Fig. 13. Frequency distribution of time needed to solve the optimal control problem, depicted for each scenario $\mathcal{S}_i$, $i \in \{1, 2, \dots, 5\}$ and the entire test run $\mathcal{S}$.

to its immanent simplifications. Even though a powerful computation server was used in this work, comprehensive restrictions, e.g., limited horizon length and move blocking, were necessary to keep the computation time reasonable. Although restrictions were designed to sustain obtainable closed-loop performance, limited computation time might eventually force suboptimal solutions and lowers overall benefit. More computational power would yield better compliance with the given time limit, pushing the performance even further. Limited computational capacity in mobile applications is the most significant barrier to the proposed hybrid control scheme. Practical implementation in its presented form is realizable by providing high computational power on the refrigerated vehicle or utilizing cloud computing and appropriate communication. Especially the latter will become more economical in the future by enhanced availability of computation power and reduced operation costs. However, even at present, both approaches are in principle technically feasible.

As computation takes a significant part of the sampling time, a problem formulation is essential that accounts for the time delay between the start of the optimization and applying its solution. The presented approach considers this by assuming the plant inputs fixed for the first time step of the horizon, beginning with the first future input as a decision variable in optimization, and applying the so-calculated first future plant input at the beginning of the next step.

Besides financial expenses on hardware, license costs for optimizer algorithms have to be considered in assessing the system's practical profitability. Available (free-of-charge) alternatives to the chosen mixed-integer solver are widely discussed by Mittelmann [63]. As their performances substantially depend on the specific problem formulation [64], comprehensive comparisons are encouraged in finding a reasonable economic solution for the particular application. If a less powerful hardware and/or solver are to be used, enlarging optimization intervals and applying future input predictions, explicit control [29], or two-stage optimization [33,34] state possible remedies. As these approaches simplify the optimization problem, finding a reasonable trade-off requires a design based on comprehensive simulations.

The particular implementation approach highly depends on the eventually transported goods. While decreased food quality might not justify such efforts at the moment, application in the pharmaceutical industry with strict regulations and high product value is sensible [2]. However, rapidly advancing electrification of the transport industry and stricter emission limits favor the exploitation of system flexibility by such potent algorithms.

The implementation on a full-sized refrigerated truck needs to consider some other minor issues. Actual system characteristics and included flexibilities significantly affect attainable performance improvement over standard control approaches. Also, the availability and quality of door openings and weather predictions play a crucial role. It is highly recommended to run comprehensive simulations on a high-fidelity plant model to evaluate the economic sense for the specific application in advance.

Furthermore, providing necessary measurements may prove challenging in a practical application. Besides the additional costs and risk of failure, the proposed sensor position inside the cooling chamber is prone to error in the harsh transportation business. A possible remedy in the form of a temperature estimator that relies only on already mounted sensors exists in literature [37] but comes with additional parameterization and implementation effort.

Due to the specifically chosen performance objective, this work considers closed-loop stability empirically. An analytic stability proof entails further research. Especially the chosen input blocking [47] complicates approaches presented in the literature [45,65]. If an analytic proof is needed, the authors recommend adapting the objective function so that asymptotic closed-loop stability is guaranteed upfront. However, this impedes a real-time capable multi-objective optimization of temperature and efficiency aspects and is therefore excluded from the given work.

8. Conclusion

This work presents an advanced holistic control scheme for the refrigeration system of a cooling truck. In essence, it is based on the well-studied hybrid model predictive control (HMPC) theory but appropriately adapted to fulfill the specific application's needs in the best possible way. Therefore, full utilization of the operational flexibility is enabled by incorporating a comprehensive hybrid model, on which the authors elaborated in a previous work [19], into the optimization task. That means it, in contrast to existing approaches, gets along without a priori heuristic simplifications, explicitly considers changes in system dynamics, and includes all manipulated inputs as independently controllable. Additionally, introducing a permissible temperature window, a modular objective function including efficiency aspects, and constraints reducing the computational burden but sustaining flexibility for the better part allow real-time operation aiming at minimal energy consumption while maintaining crucial temperature restrictions. These extensions constitute the novel contribution of this work to control design. Although focused on secondary loop refrigeration units in small-scale applications, the proposed findings still hold qualitatively for classic cooling units and systems of different sizes.

Comparisons with a classic model predictive approach (MPC) and a simple proportional–integral (PI) controller allow for a reasonable performance assessment. While the MPC is a less flexible version of the HMPC and is deduced by applying vast simplifications, the PI scheme represents the standard in industrial applications and serves as the performance baseline. Comparative closed-loop experiments were conducted on a specifically designed test bed [21] using a test run (data length: 6.25 h) representative for practical operation. They state another novel contribution of this work since no literature has reported on such a comprehensive and methodical experimental comparison. These tests verify the HMPC's superiority. It clearly outperforms standard control schemes, represented by energy savings of 16.4% and increased temperature performance of 3.4% compared with the PI-controlled case. It is especially advantageous when door openings are known upfront, for which the HMPC achieves a reduction in energy consumption of 29.6%. Even in pull-down operation, the HMPC effects energy savings of 5.0%. Although the classic MPC attains a similar energy performance, significant temperature deviations indicate that the hybrid formulation is crucial to optimally harnessing the system's intrinsic flexibility potential.

Besides the obvious advantages of reduced operating costs and loss of goods due to otherwise poor temperature conditions, such a scheme offers further benefits. The optimization-based formulation allows for a simple and intuitive way of adapting the closed-loop behavior. With changing weighting factors in the performance objective, one can directly affect the energy-temperature trade-off according to application needs. Furthermore, other system dynamics or extensions can be accounted for by simply replacing the model formulation. This further stresses the HMPC's broad applicability and capacity.

Although the proposed method faces computational challenges, the energy and temperature performance increase outweigh the additional design effort by far. Therefore, it constitutes a well-suited method for lowering the economic costs and ecological impact of refrigerated last-mile transportation.

Declaration of competing interest

The authors declare that they have no known competing financial interests or personal relationships that could have appeared to influence the work reported in this paper.

Data availability

Data will be made available on request.

Acknowledgments

This work was supported by the Austrian Research Promotion Agency (Forschungsförderungsgesellschaft) by the project *DiNaMiC* [grant number 871303].

The authors acknowledge TU Wien Bibliothek for financial support through its Open Access Funding Programme.

Appendix A. Specifications of the experimental setup

Table A.1 summarizes the specifications of the test bed's hardware components.

Table A.1
Specifications of the experimental setup.

Element	Value
Cooling chamber	
Dimensions	400 mm × 585 mm × 770 mm
Volume	180 l
Cooling unit	
Peltier element	ET-161-12-08-E [53]
Heat sink	Fischer LA V 6-100-24 [66]
Fan	ebm-papst 614 NHH-119 [67]
Peltier actuation (buck converter)	
Supply voltage	24 V
Period	50 ms
Switch	HandsOn Tec BTS7960 [68]
Inductance	200 µH
Capacity	44 µF
Diode	SB1245
Fan actuation	
Relay	SONGLE RELAY SRD-05VDC-SL-C [69]
Data acquisition	
Sampling time	2.5 s
Setup for $\vartheta_s, \vartheta_{cc}, \vartheta_{amb}, \vartheta_{wtr}$	
Sensor	Dallas DS18B20 [70]
Transducer	Artekit Labs DS2482-100 [71]
Accuracy	±0.5 °C
Setup for I_{cl}	
Sensor	Adafruit INA260 [72]
Accuracy	±0.5%
Setup for P_{cl}, P_f	
Sensor	Adafruit INA260 [72]
Accuracy	±0.9%
Setup for s_d	
Sensor	RS Pro AP5T31Z11 [73]
Computation	
Local computation unit	
Used for	PI controller, MPC
Processor	Intel Core i7-10510U [74]
RAM	16 GB
Computation server	
Used for	HMPC
Processor	Intel Core i9-10850K [75]
RAM	32 GB

Appendix B. Numerical values of model parameters

Estimated means and standard deviations of model parameters (14) are presented in Table B.1.

Regarding the affine approach (23), Table B.2 gathers chosen validity limits and associated coefficients with their estimated mean and 95% confidence interval.

Appendix C. Numerical values of control parameters

The control parameters introduced in Section 4 and settings related to the utilized solver, i.e., Gurobi [50], are chosen for the specific application according to Table C.1.

Table B.1
Estimated model parameter values.

Parameter	Estimated value	Unit
α_1	0.113 (±0.14%)	$\mathrm{W\,A^{-1}\,K^{-1}}$
α_2	2.26 (±0.02%)	$\mathrm{W\,A^{-2}}$
α_3	1.90 (±0.30%)	$\mathrm{W\,K^{-1}}$
β	1130 (±0.33%)	$\mathrm{W\,s\,K^{-1}}$
γ_1	7.31 (±0.28%)	$\mathrm{W\,K^{-1}}$
γ_2	0.606 (±0.50%)	$\mathrm{W\,K^{-1}}$
ζ	6.04 (±0.05%)	W
κ_1	11500 (±0.40%)	$\mathrm{W\,s\,K^{-1}}$
κ_2	5.30 (±0.67%)	$\mathrm{W\,K^{-1}}$
ξ_1	1.09 (±0.36%)	$\mathrm{W\,K^{-1}}$
ξ_2	15.4 (±0.46%)	$\mathrm{W\,K^{-1}}$
χ	4220 (±0.47%)	$\mathrm{W\,s\,K^{-1}}$

Table B.2
Validity limits and estimated coefficients.

Parameter	(Estimated) value	Unit
$\underline{I}_{\mathrm{cl}}^{\mathrm{af}}$	3.0	A
$\bar{I}_{\mathrm{cl}}^{\mathrm{af}}$	7.0	A
$\underline{\vartheta}_{\mathrm{s}}^{\mathrm{af}}$	−7.5	°C
$\bar{\vartheta}_{\mathrm{s}}^{\mathrm{af}}$	17.5	°C
λ_1	0.565 (±4.3%)	$\mathrm{W\,K^{-1}}$
λ_2	8.68 (±1.8%)	$\mathrm{W\,A^{-1}}$
λ_3	103 (±6.6%)	W
λ_4	19.4 (±0.8%)	$\mathrm{W\,A^{-1}}$

Table C.1
Control parameter values.

Parameter	Value	Unit
General		
t_{s}	20	s
$\vartheta_{\mathrm{cc}}^{\mathrm{ref}}$	5.0	°C
$\vartheta_{\mathrm{tw}}^{\mathrm{min}}$	4.5	°C
$\vartheta_{\mathrm{tw}}^{\mathrm{max}}$	5.5	°C
$I_{\mathrm{cl}}^{\mathrm{min}}$	3.0	A
$I_{\mathrm{cl}}^{\mathrm{max}}$	7.0	A
$\tau_{\{\mathrm{cl,\ f}\}}^{\{\mathrm{on,\ off}\}}$	100	s
PI related		
K_{p}	−2	$\mathrm{A\,K^{-1}}$
t_{n}	200	s
Observer related		
$\hat{\mathbf{x}}_{\mathrm{C}}(\text{-}1)$	$293.15 \cdot \mathbf{1}_{3\times1}$	K
$\hat{\mathbf{P}}(\text{-}1)$	diag [9, 12, 1, 9, 12]	$\mathrm{K^2}$
$\boldsymbol{Q}_{\mathrm{x}}$	diag [1, 1, 0.01]	$\mathrm{K^2}$
$\boldsymbol{Q}_{\mathrm{d}}$	diag [1, 1]	$\mathrm{K^2}$
$\boldsymbol{Q}_{\mathrm{y}}$	diag [1, 1]	$\mathrm{K^2}$
HMPC/MPC related		
N_{C}	30	Steps
N_{p}	59	Steps
$\vartheta_{\mathrm{tw}}^{\mathrm{sm}}$	5.3	°C
$\vartheta_{\mathrm{s}}^{\mathrm{min}}$	−10	°C
R_{im}	10^3	1
$R_{\mathrm{tt}}^{\mathrm{abs}}$	$5 \cdot 10^3$	1
$R_{\mathrm{tt}}^{\mathrm{sq}}$	10^3	1
R_{ec}	5	1
R_{tw}	400	1
$t_{\mathrm{d}}^{\mathrm{unexp}}$	120	s
$\boldsymbol{r}_{\mathrm{mb}}$	$[1, 2, \ldots, 29]$	–
$\mathbf{c}_{\mathrm{mb}}$	$[1, 2, \ldots, \overbrace{10, \ldots, 10}^{5\times}, \underbrace{11, \ldots, 11}_{5\times}, \underbrace{12, \ldots, 12}_{10\times}]$	–
Gurobi related		
Version	9.5.2	–
MIPFocus	3	–
Cuts	1	–
Time limit	18	s

References

[1] R. Jedermann, U. Praeger, M.G. Leibniz, W. Lang, Temperature deviations during transport as a cause for food losses, in: Preventing Food Losses and Waste To Achieve Food Security and Sustainability, Burleigh Dodds Science Publishing, 2020, pp. 301–340.

[2] N. Barrowclough, The cost of a broken cold chain in the pharmaceutical industry, 2020, https://pharma-mon.com/drug-storage-monitoring/. (Accessed 06 February 2023).

[3] Food and Agriculture Organization of the United Nations, Global food losses and food waste–extent, causes and prevention, 2011, http://www.fao.org/3/mb060e/mb060e00.htm. (Accessed 06 February 2023).

[4] O. Adekomaya, T. Jamiru, R. Sadiku, Z. Huan, Sustaining the shelf life of fresh food in cold chain – A burden on the environment, Alex. Eng. J. 55 (2) (2016) 1359–1365, http://dx.doi.org/10.1016/j.aej.2016.03.024.

[5] UNEP, Report of the refrigeration, air conditioning and heat pumps Technical Options Committee (RTOC), 2010.

[6] S. Tassou, G. De-Lille, Y. Ge, Food transport refrigeration – Approaches to reduce energy consumption and environmental impacts of road transport, Appl. Therm. Eng. 29 (8) (2009) 1467–1477, http://dx.doi.org/10.1016/j.applthermaleng.2008.06.027.

[7] P. Artuso, S. Marinetti, S. Minetto, D.D. Col, A. Rossetti, Modelling the performance of a new cooling unit for refrigerated transport using carbon dioxide as the refrigerant, Int. J. Refrig. 115 (2020) 158–171, http://dx.doi.org/10.1016/j.ijrefrig.2020.02.032.

[8] P. Glouannec, B. Michel, G. Delamarre, Y. Grohens, Experimental and numerical study of heat transfer across insulation wall of a refrigerated integral panel van, Appl. Therm. Eng. 73 (1) (2014) 196–204, http://dx.doi.org/10.1016/j.applthermaleng.2014.07.044.

[9] H. Assellaou, O. Souissi, M. Assellaou, F. Mougli, A logistic 4.0: A review of optimal temperature control problems in refrigerated transport systems, in: 2021 1st International Conference on Cyber Management and Engineering, CyMaEn, 2021, pp. 1–6, http://dx.doi.org/10.1109/CyMaEn50288.2021.9497306.

[10] M. Liu, W. Saman, F. Bruno, Development of a novel refrigeration system for refrigerated trucks incorporating phase change material, Appl. Energy 92 (2012) 336–342, http://dx.doi.org/10.1016/j.apenergy.2011.10.015.

[11] P. Gao, L. Wang, F. Zhu, Vapor-compression refrigeration system coupled with a thermochemical resorption energy storage unit for a refrigerated truck, Appl. Energy 290 (2021) 116756, http://dx.doi.org/10.1016/j.apenergy.2021.116756.

[12] K. Wang, M. Eisele, Y. Hwang, R. Radermacher, Review of secondary loop refrigeration systems, Int. J. Refrig. 33 (2) (2010) 212–234, http://dx.doi.org/10.1016/j.ijrefrig.2009.09.018.

[13] Q. Liu, Z. Sun, Q. Wang, X. Bai, C. Su, Y. Liang, S. Tian, H. Sun, J. Peng, S. Liu, S. Dong, K. Hu, Influence of secondary fluid on the performance of indirect refrigeration system, Appl. Therm. Eng. 197 (2021) 117388, http://dx.doi.org/10.1016/j.applthermaleng.2021.117388.

[14] J.-P. Rodrigue, The Geography of Transport Systems, Routledge, London, 2020, p. 480, http://dx.doi.org/10.4324/9780429346323.

[15] M. Shanks, N. Jain, Control of a hybrid thermal management system: A heuristic strategy for charging and discharging a latent thermal energy storage device, in: 2022 21st IEEE Intersociety Conference on Thermal and Thermomechanical Phenomena in Electronic Systems, ITherm, 2022, pp. 1–10, http://dx.doi.org/10.1109/iTherm54085.2022.9899546.

[16] J. Fasl, Modeling and Control of Hybrid Vapor Compression Cycles, Master's thesis, University of Illinois at Urbana-Champaign, 2013, http://hdl.handle.net/2142/45429.

[17] T. Lafaye De Micheaux, M. Ducoulombier, J. Moureh, V. Sartre, J. Bonjour, Experimental and numerical investigation of the infiltration heat load during the opening of a refrigerated truck body, Int. J. Refrig. 54 (2015) 170–189, http://dx.doi.org/10.1016/j.ijrefrig.2015.02.009.

[18] S. James, C. James, J. Evans, Modelling of food transportation systems – A review, Int. J. Refrig. 29 (6) (2006) 947–957, http://dx.doi.org/10.1016/j.ijrefrig.2006.03.017.

[19] M. Fallmann, A. Poks, M. Kozek, Control-oriented hybrid model of a small-scale refrigerated truck chamber, Appl. Therm. Eng. 220 (2023) 119719, http://dx.doi.org/10.1016/j.applthermaleng.2022.119719.

[20] F. Borrelli, A. Bemporad, M. Morari, Predictive Control for Linear and Hybrid Systems, Cambridge University Press, 2017, http://dx.doi.org/10.1017/9781139061759.

[21] M. Fallmann, J. Kölbl, T. Ausweger, M. Lösch, A. Poks, M. Kozek, Test bed emulation of secondary loop refrigeation units using peltier elements: An impedance control approach, in: 22nd IFAC World Congress, July 9-14 2023, Yokohama, Japan, 2023.

[22] J. Rawlings, D. Mayne, Model Predictive Control: Theory and Design, Nob Hill Publishing, LLC, 2009.

[23] E. Luchini, D. Radler, D. Ritzberger, S. Jakubek, M. Kozek, Model predictive temperature control and ageing estimation for an insulated cool box, Appl. Therm. Eng. 144 (2018) 269–277, http://dx.doi.org/10.1016/j.applthermaleng.2018.08.045.

[24] S.E. Shafiei, A. Alleyne, Model predictive control of hybrid thermal energy systems in transport refrigeration, Appl. Therm. Eng. 82 (2015) 264–280, http://dx.doi.org/10.1016/j.applthermaleng.2015.02.053.

[25] E. Luchini, A. Poks, D. Radler, M. Kozek, Model predictive temperature control for a food transporter with door-openings, in: 2020 SICE International Symposium on Control Systems, SICE ISCS, 2020, pp. 85–91, http://dx.doi.org/10.23919/SICEISCS48470.2020.9083491.

[26] Y. Huang, A. Khajepour, F. Bagheri, M. Bahrami, Optimal energy-efficient predictive controllers in automotive air-conditioning/refrigeration systems, Appl. Energy 184 (2016) 605–618, http://dx.doi.org/10.1016/j.apenergy.2016.09.086.

[27] A. Aliu, M.-S. Imran, T.Q. Dinh, J. Yoon, Thermal management of refrigeration unit for electric refrigerated vans: An experimental case study, Energy Rep. 8 (2022) 848–856, http://dx.doi.org/10.1016/j.egyr.2022.10.269, 2022 The 5th International Conference on Renewable Energy and Environment Engineering.

[28] M. Morari, M. Baotic, F. Borrelli, Hybrid systems modeling and control, Eur. J. Control 9 (2) (2003) 177–189, http://dx.doi.org/10.3166/ejc.9.177-189.

[29] M. Morari, M. Barić, Recent developments in the control of constrained hybrid systems, Comput. Chem. Eng. 30 (10) (2006) 1619–1631, http://dx.doi.org/10.1016/j.compchemeng.2006.05.041, Papers form Chemical Process Control VII.

[30] L.F. Larsen, T. Geyer, M. Morari, Hybrid model predictive control in supermarket refrigeration systems, IFAC Proc. Vol. 38 (1) (2005) 313–318, http://dx.doi.org/10.3182/20050703-6-CZ-1902.00336, 16th IFAC World Congress.

[31] D. Sarabia, F. Capraro, L.F. Larsen, C. de Prada, Hybrid NMPC of supermarket display cases, Control Eng. Pract. 17 (4) (2009) 428–441, http://dx.doi.org/10.1016/j.conengprac.2008.09.003.

[32] G. Bejarano, D. Rodríguez, J.M. Lemos, M. Vargas, M.G. Ortega, MINLP-based hybrid strategy for operating mode selection of TES-backed-up refrigeration systems, Internat. J. Robust Nonlinear Control 30 (15) (2020) 6091–6111, http://dx.doi.org/10.1002/rnc.4674.

[33] H.C. Pangborn, C.E. Laird, A.G. Alleyne, Hierarchical hybrid MPC for management of distributed phase change thermal energy storage, in: 2020 American Control Conference, ACC, 2020, pp. 4147–4153, http://dx.doi.org/10.23919/ACC45564.2020.9147698.

[34] M. Mork, N. Materzok, A. Xhonneux, D. Müller, Nonlinear Hybrid Model Predictive Control for building energy systems, Energy Build. 270 (2022) 112298, http://dx.doi.org/10.1016/j.enbuild.2022.112298.

[35] Y. Ma, F. Borrelli, B. Hencey, B. Coffey, S. Bengea, P. Haves, Model predictive control for the operation of building cooling systems, IEEE Trans. Control Syst. Technol. 20 (3) (2012) 796–803, http://dx.doi.org/10.1109/TCST.2011.2124461.

[36] Product Information: Ecos M24, PRODUCTBLOKS GmbH, Korneuburg, Austria, https://pbx.at/de/products/. (Accessed 20 September 2022).

[37] M. Fallmann, A. Poks, M. Kozek, Hybrid model-based online estimation of air temperature in mobile small-scale cooling chambers, Appl. Therm. Eng. 208 (2022) 118147, http://dx.doi.org/10.1016/j.applthermaleng.2022.118147.

[38] D. Zhao, G. Tan, A review of thermoelectric cooling: Materials, modeling and applications, Appl. Therm. Eng. 66 (1) (2014) 15–24, http://dx.doi.org/10.1016/j.applthermaleng.2014.01.074.

[39] G.A. Mannella, V. La Carrubba, V. Brucato, Peltier cells as temperature control elements: Experimental characterization and modeling, Appl. Therm. Eng. 63 (1) (2014) 234–245, http://dx.doi.org/10.1016/j.applthermaleng.2013.10.069.

[40] G. Pannocchia, J.B. Rawlings, Disturbance models for offset-free model-predictive control, AIChE J. 49 (2) (2003) 426–437, http://dx.doi.org/10.1002/aic.690490213.

[41] D. Simon, Optimal State Estimation: Kalman, H Infinity, and Nonlinear Approaches, Wiley-Interscience, USA, 2006.

[42] C.J. Hermes, C. Melo, F.T. Knabben, J.M. Gonçalves, Prediction of the energy consumption of household refrigerators and freezers via steady-state simulation, Appl. Energy 86 (7) (2009) 1311–1319, http://dx.doi.org/10.1016/j.apenergy.2008.10.008.

[43] A. Afram, F. Janabi-Sharifi, Theory and applications of HVAC control systems – A review of model predictive control (MPC), Build. Environ. 72 (2014) 343–355, http://dx.doi.org/10.1016/j.buildenv.2013.11.016.

[44] R.E. Kalman, A new approach to linear filtering and prediction problems, ASME J. Basic Eng. 82 (1960) 35–45, http://dx.doi.org/10.1115/1.3662552.

[45] E. Camacho, D. Ramirez, D. Limon, D. Muñoz de la Peña, T. Alamo, Model predictive control techniques for hybrid systems, Annu. Rev. Control 34 (1) (2010) 21–31, http://dx.doi.org/10.1016/j.arcontrol.2010.02.002.

[46] A. Parisio, E. Rikos, L. Glielmo, A model predictive control approach to microgrid operation optimization, IEEE Trans. Control Syst. Technol. 22 (5) (2014) 1813–1827, http://dx.doi.org/10.1109/TCST.2013.2295737.

[47] R. Cagienard, P. Grieder, E. Kerrigan, M. Morari, Move blocking strategies in receding horizon control, J. Process Control 17 (6) (2007) 563–570, http://dx.doi.org/10.1016/j.jprocont.2007.01.001.

[48] MATLAB, Version R2020a, The MathWorks Inc, Natick, Massachusetts, 2020.

[49] J. Löfberg, YALMIP : A toolbox for modeling and optimization in MATLAB, in: Proceedings of the CACSD Conference, Taipei, Taiwan, 2004.

[50] Gurobi Optimization, LLC, Gurobi optimizer reference manual, 2023, URL https://www.gurobi.com.

[51] S. Mihalache, I. Flamaropol, F.-S. Dumitru, L. Dobrescu, D. Dobrescu, Automated cooling control system through Peltier effect and high efficiency control using a DC-DC Buck converter, in: 2015 International Semiconductor Conference, CAS, 2015, pp. 281–284, http://dx.doi.org/10.1109/SMICND.2015.7355233.

[52] R. Rakhmawati, J. Hilmyvarafi Farrasbyan, Suhariningsih, F. Dwi Murdianto, Performance robustness of PID controller in buck converter for cooling system, in: 2018 International Seminar on Application for Technology of Information and Communication, 2018, pp. 127–132, http://dx.doi.org/10.1109/ISEMANTIC.2018.8549781.

[53] Datasheet: Peltier Module ET-161-12-08-E, European Thermodynamics Ltd, Leicestershire, United Kingdom, https://at.rs-online.com/web/p/peltiermodule/6935107. (Accessed 04 February 2023.

[54] DIN 19227-2: Graphische Symbole und Kennbuchstaben für die Prozeßleittechnik, Darstellung von Einzelheiten, 1991, DIN 19227-2.

[55] K. Åström, T. Hägglund, PID Controllers: Theory, Design, and Tuning, ISA - The Instrumentation, Systems and Automation Society, 1995.

[56] L. Wang, Model Predictive Control System Design and Implementation using MATLAB, Springer, London, 2009.

[57] L. Grüne, J. Pannek, M. Seehafer, K. Worthmann, Analysis of unconstrained nonlinear MPC schemes with time varying control horizon, in: 2012 IEEE 51st IEEE Conference on Decision and Control, CDC, 2012, pp. 2605–2610, http://dx.doi.org/10.1109/CDC.2012.6426581.

[58] F. Di Palma, L. Magni, On optimality of nonlinear model predictive control, Systems Control Lett. 56 (1) (2007) 58–61, http://dx.doi.org/10.1016/j.sysconle.2006.07.011.

[59] Y. Huang, A. Khajepour, F. Bagheri, M. Bahrami, Modelling and optimal energy-saving control of automotive air-conditioning and refrigeration systems, Proc. Inst. Mech. Eng. D 231 (2016) http://dx.doi.org/10.1177/0954407016636978.

[60] C.O. Negrão, C.J. Hermes, Energy and cost savings in household refrigerating appliances: A simulation-based design approach, Appl. Energy 88 (9) (2011) 3051–3060, http://dx.doi.org/10.1016/j.apenergy.2011.03.013.

[61] W.J. Cole, T.F. Edgar, A. Novoselac, Use of model predictive control to enhance the flexibility of thermal energy storage cooling systems, in: 2012 American Control Conference, ACC, 2012, pp. 2788–2793, http://dx.doi.org/10.1109/ACC.2012.6314689.

[62] A. Raval, S. Solanki, R. Yadav, A simplified heat transfer model for predicting temperature change inside food package kept in cold room, J. Food Sci. Technol. 50 (2013) 257–265, http://dx.doi.org/10.1007/s13197-011-0342-z.

[63] H. Mittelmann, Decision Tree for Optimization Software, 2023, http://plato.asu.edu/bench.html. (Accessed 22 June 2023).

[64] C. Kirches, Fast Numerical Methods for Mixed-Integer Nonlinear Model-Predictive Control, Springer Fachmedien, Wiesbaden, 2011, http://dx.doi.org/10.1007/978-3-8348-8202-8.

[65] M. Lazar, W.P.M.H. Heemels, S. Weiland, A. Bemporad, Stabilizing model predictive control of hybrid systems, IEEE Trans. Automat. Control 51 (11) (2006) 1813–1818, http://dx.doi.org/10.1109/TAC.2006.883059.

[66] Datasheet: LA V 6-100-24, Fischer Elektronik GmbH, Lüdenscheid, Germany, https://www.fischerelektronik.de/web_fischer/de_DE/PR/LA_V6_/datasheet.xhtml;jsessionid=441B80B732743ADE29DEF50A9435A4BA?branch=K%C3%BChlk%C3%B6rper. (Accessed 04 February 2023).

[67] Datasheet: Fan 614 NHH-119, ebm-papst GmbH, Linz, Austria, https://www.ebmpapst.com/at/de/products/compact-fans/axial-compact-fans/p/614NHH119.html. (Accessed 04 February 2023).

[68] Datasheet: 43A High Power BTS7960 DC Motor Driver Module, Handson Technology Enterprise, Johor, Malaysia, https://handsontec.com/index.php/product/43a-high-power-bts7960-dc-motor-driver-module/. (Accessed 04 February 2023).

[69] Datasheet: SRD-05VDC-SL-C, Ningbo Songle Relay Co.,ltd, Zhejiang, China, https://datasheetspdf.com/pdf-file/720556/Songle/SRD-05VDC-SL-C/1. (Accessed 04 February 2023).

[70] Datasheet: Dallas DS18B20, Otom Group GmbH, Bräunlingen, Germany, https://www.sensorshop24.de/kabelfuehler-durchmesser-6mm. (Accessed 24 February 2023).

[71] Datasheet: DS2482-100, Artekit Labs, Porto Recanati, Italy, https://www.artekit.eu/products/breakout-boards/io/ak-ds2482s-100/. (Accessed 04 February 2023).

[72] Datasheet: INA260, Adafruit Industries, New York City, USA, https://learn.adafruit.com/adafruit-ina260-current-voltage-power-sensor-breakout. (Accessed 04 February 2023).

[73] Datasheet: Limit Switch, RS Components GmbH, Frankfurt, Germany, https://de.rs-online.com/web/p/endschalter/9026871?sra=pmpn. (Accessed 04 February 2023).

[74] Datasheet: i7-10510U, Intel Corporation, CA, USA, https://www.intel.com/content/www/us/en/products/sku/196449/intel-core-i710510u-processor-8m-cache-up-to-4-90-ghz/specifications.html. (Accessed 04 February 2023).

[75] Datasheet: i9-10850K, Intel Corporation, CA, USA, https://www.intel.com/content/www/us/en/products/sku/205904/intel-core-i910850k-processor-20m-cache-up-to-5-20-ghz/specifications.html. (Accessed 04 February 2023).